Once and Future Forests: Historical Reconstructions and Climate Change Experiments for California Pines and Oaks

By

PAIGE VENICE KOUBA
DISSERTATION

Submitted in partial satisfaction of the requirements for the degree of

DOCTOR OF PHILOSOPHY

in

Ecology

in the

OFFICE OF GRADUATE STUDIES

of the

UNIVERSITY OF CALIFORNIA

DAVIS

Approved:

_____

Andrew M. Latimer, Chair

_____

Malcolm P. North

_____

Susan P. Harrison

_____

Matthew E. Gilbert

_____

Xiaoli Dong

Committee in Charge

2024

Abstract

California's forests are beset by multiple threats from climate change, including increased fire and drought severity. A single tree can be thought of as a victim to the influences of its climate, at risk of mortality from any number of climate-related stresses. However, forests collectively are a key determinant of some of the very same processes that lead to these risks. In order to effectively manage forest ecosystems and support the human communities that live in and near them, we must examine the causes and effects of forest patterns and process, across scales of space and time.

The spatial structure of a forest—the size and arrangement of its constituent trees—can be more or less resistant and resilient to wildfire. Fire in turn can, abruptly or gradually, shape a forest structure towards more heterogeneous stands, which are well adapted to frequent, low-intensity fire. The era of fire exclusion (staring around 1850) has prevented this self-regulating feedback from taking place, leading to crowded, homogeneous forest stands, with high fuel loads that make them vulnerable to stand-replacing fires. Studying the forest structure from a time before the end of frequent, low-intensity fire can give managers a reliable target for the spatial and structural characteristics of a fire-adapted forest. We apply dendrochronological reconstruction methods to Jeffrey pine (*Pinus jeffreyi*) forests in the Eastern Sierra Nevada, in order to estimate the conditions of fire-adapted forests specific to this region. This is the first spatially explicit stand reconstruction study to take place in the Eastern Sierra, which experiences a unique climate and fire regime compared to its more mesic western-slope counterpart. We present findings indicating that Eastern Sierra stands have increased in density, with fewer trees existing as singletons and fewer, smaller gaps between clumps of trees. But our results also indicate that as few as one to two moderate-severity fires (prescribed fire or wildfire) can meaningfully restore this forest type to its fire-adapted state.

California's forests and woodlands can change gradually, as they did through hundreds of years of fire suppression; or they can change rapidly, as seen in the waves of mortality caused by the state's 2012-2017 drought. Water stress, whether cumulative or acute, has always been and will always be one of

the greatest challenges to terrestrial plant life. Because plants lose water through their leaves in the process of acquiring CO_2 for photosynthesis, it is thought that rising atmospheric CO_2 levels could ameliorate the effects of water stress in trees, allowing them to reduce their water losses while increasing their net CO_2 uptake. We wished to investigate whether, how, or to what extent high CO_2 levels help the youngest trees endure or avoid water stress. Using a newly constructed free-air CO_2 enrichment (FACE) system at Quail Ridge Reserve, we planted 384 acorns of two native California oak species (*Quercus lobata* and *Q. wislizeni*) directly into the soil. We subjected half of the seedlings to continuous treatment with elevated CO_2 (ambient + 137 ppm). Half of the seedlings received supplemental water during the summer. These two factors were combined to yield four treatment levels. By comparing the differences between well-watered and under-watered plants at ambient CO_2 vs. elevated CO_2, we were able to test for interactions between the CO_2 treatment and the watering treatment. We found that in the cases where watering's effect differed by CO_2 treatment, it was only the well-watered seedlings that benefited from the extra CO_2 (for *Q. wislizeni*, the benefit came in the form of increased photosynthetic rates; for *Q. lobata*, the benefit was an increase in post-grazing resprouting rates). This result may indicate that future climates will widen, rather than narrowing, the fitness gap between oak seedlings with access to abundant water, and those without it.

Table of Contents

Land Acknowledgement

I conducted my dissertation research at the University of California, Davis, which was built in the ancestral homeland of the Patwin people. The story of native oaks, and the current threat of their regeneration failure, is inextricably tied with the story of the oppression of the Central Valley's Patwin and Miwok tribes, who have relied on acorns as a food source and cultural touchstone for generations. My fieldwork also took me to the lands long tended and still cared for by the Mono Lake Kutzadika'a, who turned to the Jeffrey pines for *piagi*, a food source which families harvested together from the very same forests featured in these pages (Slaton et al. 2019). That land itself, as well as the land where my research on oak seedlings occurred, and the land that is now UC Davis Campus, was seized by unratified treaty in the spring and summer of 1851 (Lee 2020)

In the six years I have spent working on my PhD, I have tried my best to learn something worth sharing about the California ecosystems that I have made my home in. I know that I walk in the footsteps of greater and deeper knowledge, held not only by individuals but by entire cultures. I have also sought to learn about the original inhabitants of this land and the government-sanctioned slaughter they endured, and which untold thousands did not survive (Madley 2016). The settler-colonizer tradition that is my heritage has been disastrous for the health and survival of California's ecosystems and native peoples.

Acknowledgements

If I have learned one thing from my time in Davis, it is that research is much better when done with people. My quality of life, and my skill as a scientist, have both increased in direct proportion to the number of friends I've had the gift of meeting along the way. So believe me when I say that I could fill another eighty-page document with my gratitude.

To begin with, I couldn't have completed any of these projects without help from the following kind souls: (Chapter 1) Derek Churchill, Andrew Sánchez-Meador, Marc Meyer; (Chapter 2) Tom Buckley, Ross Brennan, Adam Spyres, Shane Waddell; (Chapter 3) Dave Muffly and Dave Teuschler. My father, Patrick Kouba, built the best weatherproof hutch a field ecologist daughter could ask for. Adriana Postema, if you hadn't helped me to build vole-cages for eight hours on the hottest day of the year, I wouldn't have had anything left to write about.

I thank my advisors, Dr. Andrew Latimer and Dr. Malcolm North. Though I should have scheduled more of them, I came away from every meeting with Malcolm feeling reinvigorated about the challenges of the work, and thankful for his affable attitude and hard-won widsoms. Andrew, thank you for your faith in me and your constant efforts to know and love the world even better. I will miss our check-in meetings and their philosophical tangents and wild, rapid-fire stories.

I am deeply grateful to my other *three* committee members—there's a good reason I chose to have the maximum allowable number to sign off. Dr. Susan Harrison did me the service of always expecting my best, and she made me better for it. Dr. Matthew Gilbert was so incredibly generous with his time and mentorship in building the FACE system that I sometimes forgot this whole academia thing is supposed to be a rat race. Dr. Xiaoli Dong can make the most intimidating concepts in our field seem not only understandable but irresistibly fascinating; she has the gift of sharing her brilliance in a way that somehow makes you feel smarter, too.

The whole Latimer + North + FOCAL + Friends super-lab has gotten me through many a hard day. I have loved every moment I've gotten to spend in the web of mentoring, collaboration, and

friendship we all built together. Marina, Joan, Allie, Derek, Quinn, Jan, Max: thank you for helping lift up your newer lab mates. Nina, Emily, Jenny, Hilary, Anjum, I will miss you all terribly when I finally go.

To all my students, in Kenya, Cambridge, Petersham, Davis, and anywhere in between: Thank you for sharing your curiosity with me. Learning from you and with you is my greatest privilege.

A special thank-you to Jill Dyer, Ian Clark, Sarah Perry, Hattie Hughes, and Saaniya Patwardhan, for being my intrepid collaborators in research. It's time I told you, I have no idea what I'm doing at all. But your enthusiasm, helpfulness, and ability to roll with the punches made the confusion fun.

Ellie, Alex, and Liza, I'm so glad I bumped into you as we all found our way to someplace. I am a better person for our friendship, and I will always count myself lucky to have friends who live their lives with such courage, kindness, community engagement and deep meaning.

I am grateful to: Beshara Kehdi and Joanna Wirkus, for co-leading the best radical pedagogy community I have ever had the privilege of participating in; Ken Shindledecker for inspiring my love of ecology; Dr. Tony Kiszewski for being a dear friend and mentor all these years; Dr. Dan Schrag and Dr. Lauren Kuntz for being the kind of people I decided I wanted to be around, and helping me apply to grad school to seek them out; Brian, for sticking with me all these years and all the ones to come; Charlie, for encouraging and helping me to better love and embrace all the different mes; All the members of Chrome Toaster, the best band I have ever been in; My Davis running/life-ing pals: Clancy, for setting the pace, Nathan for sharing the miles, and Sarah, Jen, and Jonah for singing the praises of Grocery Outlet; Coach John and the whole Davis Tri team; Dr. Laci Gerhart for modeling the kind of teaching that changes lives, and telling the kind of jokes that do, too; Emma Forester and Isabela Alvarez, for making Davis a home.

To my family. Mom, thank you for always being a call away. Dad, thank you for helping me learn how to fix things. Claire and Eric, I don't know how many hours you spent with me in advice and problem-solving sessions, but I promise to pay it forward one day. Katie, thank you for your good heart and beautiful letters. Grace, thank you for reminding me that the bells and whistles are not what matter about people, and that it is okay to fail.

Adriana, you are my best and I'm so lucky you came into my life.

Introduction

Researchers can have several different goals in mind when they set out to study forest ecosystems. Often, we aim to conserve forests where they are whole, and restore them where they are not. To practice restoration most often involves looking to the past for a reference condition of a fully functioning forest (Urgenson et al. 2018), and indeed knowledge of the history of California's forests are critical to proper research, management, and appreciation of them. Many forest restoration projects seek to repair the damage done by climate-related stresses (e.g. fire, heatwaves, drought). But although every tree is subject to those threats, forests also collectively help determine the direction the changing climate will take, as a critical part of the exchange of CO_2 between the atmosphere and the biosphere. Understanding trees and forests is therefore necessary to understanding the future of our planet and its climate. Without knowing the history of forests, we enter an uncertain future with no map. Without acknowledging that climate change is altering the patterns and processes that make up a forest, we risk relying on a map that is wrong.

The following chapters will reach back decades into the past, to examine historical forest conditions in the early 1940s; and they will attempt to peer into the future, using elevated CO2 to subject tree seedlings to the climate conditions predicted for the mid-to-late 21st Century.

Beginning in the 1850s, the suppression of indigenous cultural burning and naturally occurring wildfires alike became the policy of forest managers in the western United States (Taylor et al. 2016). In California, this fire exclusion era has fundamentally reshaped many parts of the forest, increasing density, homogenizing tree sizes and ages, and increasing fuel loads (Lydersen et al. 2013, Safford and Stevens 2017). But not all forests respond to fire deficit in identical ways. Much research on the effects of fire suppression has focused on the mesic, productive slopes of the Western Sierra. Fire deficit in Western Sierra forests has caused an accumulation of surface fuels, rendering present forests more vulnerable to climate-driven increases in fire severity and size (Hagmann et al. 2021). Eastern Sierra Jeffrey pine forests, however, feature a distinct climate and fire regime from that of their Western Sierra mixed-

conifer counterparts (North et al. 2009), necessitating a separate evaluation of fire exclusion's effect on their density and spatial characteristics. Stand structure is important to forest health, function, and fire dynamics (Larson and Churchill 2012, Koontz et al. 2020, Ma et al. 2023), but until now no studies have applied spatially explicit historical analysis to forests in the Eastern Sierra.

Forest stands are partly shaped by fire regimes, and forest structural characteristics also have a role in determining future fire occurrence (Agee 1996), in a dynamic feedback between pattern and process (Larson and Churchill 2012). Spatially complex forests provide low surface fuels in openings, reducing radiant and convective heat which otherwise might support a high-severity crown fire (Graham et al. 2004). Within modern forests, more heterogeneous stand structure has been shown to promote resistance and resilience to fire (Koontz et al. 2020), and restoring forests to the spatial and structural pattern they maintained prior to the fire exclusion era can help them support and re-adapt to frequent, low-intensity fire (Fry et al. 2014). Results from Chapter 1 indicate that just one to two moderate-severity fires can meaningfully restore an Eastern Sierra pine forest to pre-fire-exclusion conditions, which may be better suited to withstand frequent low-severity fires.

Fire exclusion is just one of the many dramatic changes humans have brought to bear on California forests in the last two centuries. In the time it took to turn pre-settlement forests into the crowded, homogeneous stands seen today, atmospheric CO_2 levels increased from 280 to over 420 ppm (Gulev et al. 2021). In the past 30 years, much progress has been made in researching how this gradual increase has changed conditions for plant life, in particular with the development of free-air CO_2 enrichment (FACE) research (Ainsworth and Long 2021). This field-based method allows for the observation of plants responding to elevated CO_2 levels in natural conditions, as opposed to in labs and growth chambers. FACE has provided a unique opportunity to experimentally examine the way plants behave under conditions predicted for the coming decades. Chapter 2 presents a novel FACE-like experimental array, designed for studying the effects of elevated CO_2 on short-stature plants. "TinyFACE" is an inexpensive, modular, and customizable option for climate change research in plants.

Thanks in part to FACE research, the first-order effects of future CO_2 levels are increasingly well understood (Ainsworth and Long 2021). Research efforts are now largely focused on the interaction of elevated CO_2 with one or more additional environmental variables (Way et al. 2015), especially those known to also be changing due to climate change, like soil water availability.

Trees take up water through their roots and lose it through their leaves via their leaf pores, which can regulate this loss by reducing their openness in response to stress (Xu et al. 2016). These pores, called stomata, are also the entry point through which all plants must take in CO_2, the feedstock of photosynthesis, to convert into sugars and living tissue (Lambers et al. 2008). Since CO_2 enters the leaf and water exits the leaf through the same gateway (Woodward 1987), a common understanding is that elevated CO_2 will allow plants to reduce water loss, thereby increasing their water use efficiency and fitness (Cernusak et al. 2019)

Elevated CO_2 is likely to influence how plants respond to environmental stressors like water shortage—in other words, present-day plant responses to familiar stressors may not be reliable in a high-CO_2 future. In fact, climate models that account for dynamic ecophysiological feedbacks in global vegetation produce meaningfully different results than models that treat plant life as a static element of the climate system (Swann et al. 2016, Anderegg et al. 2020).

The findings in Chapter 3 present a surprising scenario, in which elevated CO_2 actually exacerbates the performance gap between water-stressed and well-watered seedlings. In this case, rather than acting as a Robin Hood and preferentially offering benefits to the most down-on-their-luck seedlings, elevated CO_2 only provided a benefit to those plants that had abundant water resources with which to take advantage. Such counterintuitive findings are not rare in multi-factor climate change experiments on trees (e.g. Duursma et al. 2011, Wohlfahrt et al. 2022). They showcase the importance of directly observing plant responses to multiple interacting environmental factors, and using experiments to identify the mechanisms behind those responses.

How are we to best study and manage trees and forests? We must start by learning how disturbed forests have departed from prior, more functional states, just as we learn how stressed individuals behave

differently from plants with abundant resources. But we must undertake those inquiries with caution. As CO_2 continues to rise, as the climate continues to warm and change, novel climates and no-analog communities will become increasingly common (Williams and Jackson 2007). More and more, the past will no longer be the key to the future. Because the feedbacks between forests, fire, and climate are so important to global climate regulation and ecosystem health, we will have to find new ways to study what is to come.

Chapter 1: Prescribed and natural fire restore fire-adapted conditions in an Eastern Sierra Jeffrey pine forest

Abstract

The era of fire exclusion has had well-documented impacts on Western U.S. forests, generally leading to denser, more homogenous stands, higher proportions of shade-tolerant species, and a heightened risk of high-severity fires. Restoring forests to their historical, fire-adapted condition can ameliorate fire risk and other ecological changes, but most research on fire-adapted restoration targets in California has focused on the western slope of the Sierra Nevada mountain range. Eastern Sierra Jeffrey pine forests experience distinct climate and growth conditions from their west-side counterparts, and both their historical structure and the effects of fire suppression are different than those of their west-side counterparts. Our goals were (1) to use spatially explicit forest reconstruction methods to estimate the historical, fire-adapted structure of eastern Sierra Jeffrey pine forests; (2) to describe the structural changes observed after 54–65 years of fire exclusion; and (3) to quantify the structural effects and restoration potential of 1–2 recent fire events that followed the fire exclusion period. At two sites in the Eastern Sierra near Mammoth Lakes, CA, we surveyed stands and collected tree ring series to establish tree ages and reconstruct maps of the forest at the end of the frequent-fire period (1941), after the period of fire exclusion (1995/2006), and in recent years (2018). We found that half a century of fire exclusion led to denser stands with fewer, smaller openings and larger clumps of trees, much like in the western Sierra. However, east-side forests were not as departed from fire-adapted conditions, and 1–2 fire events in recent years showed potential to restore many structural characteristics to their prior state. Our results can inform forest management decisions, and support the use of prescribed fire and managed wildfire in the service of restoration goals.

Keywords: forest reconstruction, reference condition, Eastern Sierra, Jeffrey pine, restoration targets, individuals clumps and openings, dendrochronology

1. Introduction

In many dry conifer forests of the western US, fire exclusion has led to dramatic changes in forest structure and forest-fire feedbacks over the past century. Socioecological transitions and the resulting changes in dominant fire management practices align with marked changes in fire regime (Taylor et al. 2016). In California, natural and anthropogenic fire once maintained heterogeneous forests with low tree density and surface fuel accumulation, and a high proportion of fire-adapted species like Jeffrey pine (*Pinus jeffreyi*) (Safford and Stevens 2017). By contrast, modern California forests tend to have higher tree density, smaller trees, more even age classes and more shade-tolerant, less fire-adapted species (Dolanc et al. 2014, McIntyre et al. 2015, Safford and Stevens 2017). In addition to these well-documented changes on the landscape, fire exclusion also changes within-stand spatial structure, particularly the distribution of Individual trees, tree Clumps, and Openings—hereafter ICO, (Larson and Churchill 2012).

Fine-scale forest structural patterns are important to ecosystem functions such as drought resistance (Ma et al. 2023), habitat quality (Larson and Churchill 2012), snow retention (Churchill et al. 2013, Stevens 2017), fire resilience (Koontz et al. 2020), and inter- and intraspecies interactions, e.g. competition, facilitation, spread of disease, and recruitment (Larson and Churchill 2012). *Pinus jeffreyi* in particular requires relatively large forest openings for regeneration, as seedlings need sufficient light and soil resources to grow (Gucker 2007, Safford and Stevens 2017). Furthermore, restoring forests to the ICO pattern they maintained prior to the fire exclusion era can help them support and adapt to frequent, low-intensity fire (Fry et al. 2014). Management recommendations for fuel reduction and ecological restoration in *P. jeffreyi* forests must therefore account for ICO patterns if they are to create meaningful restoration targets. As fine-scale site features like local climate and topography have been shown to affect the arrangement of ICO patterns within a forest (Ng et al. 2020), those targets must be attuned to local and regional influences, such as the unique climate and fire regime that distinguish the Eastern Sierra from the range's more mesic western slope (North et al. 2009)

Identifying historical ICO patterns specific to frequent-fire forests in the Eastern Sierra is necessary first to characterize the modern forest's departure from fire-adapted conditions in this area, and second to set meaningful management and restoration targets. For example, the Eastern Sierra Climate and Communities Resilience Project is an ambitious 20-year management effort to restore fire-resilient landscapes in the 23,500 ha forest belt surrounding Mammoth Lakes, the largest population center in the Eastern Sierra (Pusina et al. 2023). Such projects must consider the spatial structure of a fire-adapted forest to achieve their goals, but Eastern Sierra forest managers have previously been forced to rely on studies from the Western Sierra to develop restoration and fire risk reduction targets (North et al. 2009).

Where they have taken place (Stanislaus Tuolumne NF (Lydersen et al. 2013), the Eastern Cascades (Churchill et al. 2017), Northern Arizona (Sánchez Meador et al. 2011)), forest reconstruction studies have often been limited by the long span of years elapsed since the start of fire exclusion (Lydersen et al. 2013), as early as the 1860s in most parts of the Western Sierra (Taylor et al. 2016). However, fire scar data from our study area in the Eastern Sierra record widespread forest fires until as late as 1950 (North et al. 2009). A more recent end to the frequent-fire period here has given less time for fire exclusion to influence forest structure, although forest structure variables are still mostly outside the historical natural range of variation (Meyer et al. 2019). The more recent end to frequent fire suggests that standard methods of forest reconstruction can be applied with greater-than-usual confidence in this setting. Identifying the spatial characteristics of the area's forests during the frequent-fire period provides a target structure for a more fire-adapted forest in the Eastern Sierra.

It is uncommon for forest reconstruction studies to examine the effects of fire's return, in addition to the effects of fire exclusion. Our study comprises three reference years (two reconstructed, one observed) to characterize forest conditions (1) during the active fire period, (2) after half a century of fire suppression, and (3) after the return of fire to the landscape.

The objectives of our study are (1) to use forest reconstruction methods to estimate the historical, fire-adapted structure of eastern Sierra Jeffrey pine forests; (2) to describe the structural changes observed after 54–65 years of fire exclusion; and (3) to quantify the structural effects of 1–2 recent fire events that

followed the fire exclusion period. We use tree ring series to develop an age-size regression model specific to our study area, and map the positions and estimated sizes of trees present before the end of frequent fire there in the mid-20th Century (frequent-fire reference year: 1941). Using the same methods, we reconstruct forest conditions immediately before the return of fire to the area (fire-excluded reference year: 1995 and 2006, respectively, at our two sites). Finally, we use observed modern forest conditions from our survey (modern reference year: 2018). We compare the 1941 forest to the fire-excluded forest, to determine the maximum departure from frequent-fire condition; and we compare the fire-excluded forest to the 2018 forest, to evaluate the restoration potential of 1–2 fires after decades of fire exclusion. We calculate metrics of historical, fire-excluded, and modern forest conditions such as tree density, basal area, and size distribution. We examine how the distribution and characteristics of individuals, clumps, and openings changed since the end of the frequent-fire period in the study area, and whether/to what extent those factors were restored to reference conditions by 1–2 fires in recent years. In particular, we address whether fire exclusion has affected Eastern Sierra forests in the same way and to the same extent as Western Sierra forests, with the aim to inform management restoration guidelines for a greater range of frequent-fire forest types.

2. Methods

2.1 Study Sites

Study plots were selected in August 2018, in the Inyo National Forest on the eastern slope of the Sierra Nevada, near Mammoth Lakes, California, and within the rain shadow of the mountain range (Taylor 1982). Three 1-ha circular plots were randomly chosen at each of two sites: Indiana Summit (IS), at the Indiana Summit Research Natural Area (ISNRA, 37.798247, -118.916090); and O'Harrell Canyon (OH), about 1.5 km northeast of the O'Harrell Canyon Creek Campground (37.757000, -118.746710) near Glass Mountain. The two sites, separated by appx. 15 km, share a dominant vegetation type of Jeffrey pine forest (*Pinus jeffreyi* Balf.), which makes up 99.3% of the canopy in our IS sites. OH trees were 59.6% *P. jeffreyi*, with 19.7% Sierra juniper (*Juniperus grandis*), 15.3% white fir (*Abies concolor*), and 5.4% lodgepole pine (*Pinus contorta*). Forests in the area are characterized by low recruitment rates

and long regeneration times (Taylor 1982). Plot elevation ranged from 2571 m–2615 m at IS, and 2459 m–2559 m at OH. The dominant soil types at the sites are vitrandic xerorthents (well-drained, nutrient poor, sandy soils of volcanic origin) (Esri Community Maps Contributors n.d.).

Fire reconstruction studies from the area determined a mean historic fire interval of 4.8–16.9 years (North et al. 2009) and 2–17 years (Brown et al. 2010), more frequent but overlapping with the estimate of an 11–16 year interval for this forest type in the Eastern Sierra as a whole prior to European settlement (Van de Water and Safford 2011). Natural ignitions were frequent, as the area has one of the highest lightning strike rates in the state (Wagtendonk et al. 2018). Prior to European settlement, and to a lesser extent in the 20th Century, the Bishop Paiute and Mono Lake Kutzadika'a (Northern Paiute Tribes) also practiced cultural burning in the area, including as part of a process to harvest and/or prepare the larvae of the Pandora moth (*Coloradia pandora*) as a food source (Taylor 1982, De Foliart 2002, Slaton et al. 2019). ISRNA was not logged in the 20th Century and is considered a "pristine" example of late-seral *P. jeffreyi* forest (Meyer et al. 2019). The forests around our study sites experienced frequent fire conditions from at least the late 18th Century until ca. 1950 (North et al. 2009). The middle of the 20th Century marked the start of an era with no wildfires recorded (Taylor 1982, North et al. 2009), with the exception of one lighting ignition in 1986, which was quickly suppressed (Slaton et al. 2019) and did not affect our study plots. Prescribed burn treatments took place between 1996–1998 in the northeast corner of ISRNA (Meyer et al. 2019), where our three 1-ha plots are located. Wildfire returned to the area in 2016, when the Clark Fire burned 99% of the RNA (Slaton et al. 2019), including our plots. The area of the prescribed burn treatment burned at low to moderate severity in 2016, with a composite burn severity of 20% (Meyer et al. 2019). While less historical detail is available for O'Harrell Canyon (Site OH), we assign the same date for the end of the frequent-fire period there as for IS, because the three nearest sites with fire history reconstructions all record fires into the mid-20th Century, and all three are approximately as close to OH as to IS (North et al. 2009). We were unable to find records of fire history at the O'Harrell Canyon site until 2007, when the O'Harrell Fire burned the area containing our plots at moderate severity (California Department of Forestry and Fire Protection 2019). For a conservative estimate of the fire-

adapted forest condition (i.e., the structure that existed before fire exclusion began), we chose 1941 as the focal year for our reference condition forest. We compare the reconstructed forests from 1941 to the reconstructed fire-excluded forests (1995 at IS, 2006 at OH) and the observed forests in 2018.

2.2 Sampling Methods

For each plot, we recorded position, decay class, species, and diameter at breast height (DBH) for every tree and standing snag ≥ 5 cm DBH. Downed logs were measured at their maximum diameter (used to represent DBH), and the resting place of their larger end was recorded as the tree's position. In total, we recorded 1,152 trees, logs, and snags across both sites. In addition, we cored 227 trees total using 4.3 mm increment borers (Haglöf, Inc.; Långsele, Sweden), at the lowest possible coring heights, ranging from 7–103 cm (average: 41.3 cm). For *P. jeffreyi*, the dominant species, we used a stratified random sampling technique to collect approximately 10 cores in each plot for each of three size classes: < 50 cm DBH, 51–90 cm DBH, and > 91 cm DBH. The > 91 cm size class sample was completed in August of 2019 at IS, and in May of 2021 at OH. Cores for *A. concolor* and *P. contorta* were collected from OH in June 2023. Attempts to core specimens of *J. grandis* failed due to the presence of rotten heartwood.

2.3 Tree Core Processing

Sampled cores were glued to wooden boards and sanded with progressively finer-grit sandpaper to provide a flat cross-section for reading and analysis, following standard dendrochronological methods (Stokes 1968, Speer 2010). Sanding started with 180-grit paper and a belt sander, and finished with 400-grit paper and a palm sander. We scanned each board of up to six cores at 1200 dpi (EPSON WorkForce 7610 scanner) and processed the images with CooRecorder version 7.9 (Larsson 2005) to establish ring-width series. For most cores, the pith correction tool available in CooRecorder was used to calculate the distance to pith and the estimated number of growth years represented by said distance (based on innermost ring curvature observed in the core). Forty-one rotten or unreadable cores were excluded from the sample, yielding a total of 186 cores used to conduct dendrochronological analysis (at IS, n = 88, 83.0% of cores collected; at OH, n = 98, 81.0%).

Crossdating was conducted using CDendro version 7.9 (Larsson 2005) and the dplR package in R (Bunn et al. 2024) to establish the length in years of each tree ring series. In dendrochronological analysis, a correction is necessary to account for the years of growth before the tree reached the height at which the core was taken. This core-height correction uses species-specific equations, and we used the correction equations available in the literature that most closely matched our focal species (Gascho Landis and Bailey 2006, Fraver et al. 2011, Tomiolo et al. 2016). Since *Abies concolor* is a shade-tolerant species with highly variable growth rates at the seedling and sapling stages, no core height correction was used for this species, and tree age was recorded as the number of years observed at coring height, following (Taylor and Halpern 1991).

2.4 Stand Reconstruction

We used linear age-size regressions to reconstruct tree ages in 1941, before the end of the frequent-fire period. Establishing the relationship between DBH and age allowed us to extrapolate the ages (and therefore establishment dates, and ages in 1941) for all 1,152 trees in the study. Trees were either assigned an age derived from their respective core sample (n = 157) or an age estimate from the age-size regression model (n = 995) For *P. jeffreyi*, we created separate age-size regressions for IS and OH, since their distinct topography and aspect were considered likely to cause different growth rates. For model selection, we compared corrected-AIC and BIC values for first- to fifth-degree polynomials of DBH as a predictor variable; in cases were AICc and BIC were not in agreement, we picked the more parsimonious model, since over-fitted models would perform poorly at predicting age from DBH. The resulting models had R^2 values of 0.653 and 0.646, respectively (n = 88 for *P. jeffreyi* at IS, $p << .001$; n = 79 for *P. jeffreyi* at OH, $p << .001$). Age-size regressions for *A. concolor* and *P. contorta* were established using cores from OH only, since these species represented ≤0.8% of the trees sampled at IS in 2018 (and 0% of live trees). The age-size regression for *A. concolor* had an R^2 of 0.514, and the regression for *P. contorta* had an R^2 of 0.798 (n = 10 for *A. concolor*, $p = 0.02$; n = 9 for *P. contorta*, $p = 0.003$). All models were first-degree polynomials, except for *P. contorta*, which was quadratic.

Standing snags and fallen logs ≥ 5 cm DBH were given the same diameter-based age estimate as live trees, with an additional correction for the estimated time since tree death. The age estimate and the time-since-death estimate were summed and subtracted from 2018 to determine each tree's establishment date. Time-since-death was calculated based on visually estimated decay classes (Cline et al. 1980) recorded during field surveys in 2018. We grouped the 10 decay classes into six categories (snags of class 1, snags of class 2+3, snags of class 4+5; logs of class 1, logs of class 2+3, logs of class 4+5) and populated a Leslie matrix of transition probabilities for each category based on the snag decay class transition matrix in (Morrison and Raphael 1993) (extrapolating transition probabilities from snags to logs and between classes of logs). We used this transition matrix and information on the residence time of decaying pine logs (Kueppers et al. 2004, Edelmann et al. 2023), to calculate the stable class distribution. Once the population has reached the stable class distribution, there are a finite number of pathways an individual can take to arrive at any given decay class in one five-year timestep. Therefore, for a given vector of snags/logs, it is possible to calculate the probability distribution for the decay class in the previous timestep. By iterating this process and counting the timesteps required for all trees in the starting vector to "de-age" back to the Snag Class 1 category, we were able to assign a probability distribution of the estimated number of years since death for each decay category (ranging from 5-295 years; overall mean = 99.3 years, sd = 70.3). We then drew from these distributions to assign an estimate of time-since-death to each snag and log in our 2018 dataset based on its observed decay class. These adjustments ensured that a reasonable estimate of the true establishment date for snags and logs could be assigned, in order to assess their age in past time steps. At IS, snags in Class 1 were assumed to have died in the 2016 Clark Fire, and assigned a time-since-death of two years. At OH, four logs had progressed to a state of decay that made species identification impossible; these were assigned the age estimates for *P. jeffreyi*, the most abundant species.

Using the establishment dates determined for each tree, snag, and log, we calculated each tree's age as of 1941 (for the frequent-fire reference year) and the fire-excluded reference year. We removed any trees that established after the relevant year from the dataset. Next, the reverse of the age-size

regression method above was applied to the trees' past ages, to determine DBH in past reference years. We removed any trees whose size fell below 5 cm DBH. The DBH distributions of these reconstructed forest datasets were used to calculate non-spatial metrics (trees per hectare, stand density index (SDI), quadratic mean diameter (QMD), mean DBH, and basal area (BA)) for the forest in past reference years. A t-test was used to compare each of these metrics between 1941 and fire-excluded conditions, and between fire-excluded and 2018, to establish changes in plot-level and global characteristics. Because comparisons of reconstructed stands at IS and OH revealed each site to have unique variance in initial tree size distributions, we chose to analyze changes in mean DBH on a per-site basis (IS separate from OH). Plot-level metrics were combined to increase statistical power.

2.5 Spatial Analyses

Using the stand maps of live trees from 2018, and reconstructed maps of live trees from 1941 and the fire-excluded year at each site, we were able to assess the structure of the forest in each time period, including the distribution of individual trees, clumps of trees, and openings between trees. We followed published clump detection algorithm methods (Plotkin and Muller-Landau 2002, Churchill et al. 2017). Allometries for crown projections came from (Gill et al. 2000), Table 9; *P. jeffreyi* and *J. grandis* were not included in their dataset, but we used equations for the most closely related species available (*Pinus ponderosa* and *Calocedrus decurrens*, respectively). Snags and logs observed in 2018 could be used retrospectively, to reconstruct the living trees they had once been. For the current study, we left standing dead wood out of the spatial analyses for both reconstructed and observed forest datasets.

Tree clumps were defined as groups of trees with overlapping crowns. The 1-ha plot boundary was corrected by a buffer inward from the plot edge, to minimize bias towards small clumps due to "truncated" clumps at the plot edge: any stem within the buffer was counted as a clump member, but could not form the center of a new clump. Since the average crown diameter across all plots, irrespective of time, was 4.59 m, we chose a buffer of 5 m from the plot edge, which would prevent most edge trees (trees within the buffer) from being counted incorrectly as singletons due to "invisible" out-of-bounds neighbors (Lydersen et al. 2013, Fry et al. 2014, Ng et al. 2020).

Clumps of trees and individual trees are surrounded by non-canopy area (i.e. all area in the plot not under a tree canopy), and non-canopy area is further divided into interstitial space and "openings" large enough to represent an ecologically significant interruption of the forest canopy. Openings were identified in our study using the bi0m3trics/patchwoRk package in R (Sánchez Meador 2024), an application of the PatchMorph patch delineation algorithm (Girvetz and Greco 2007). PatchMorph applies a circular kernel, based on user-defined parameters, to a landscape of mixed "suitable" and "unsuitable"-classified patches, delineating areas that function as suitable. Originally created for detecting habitat patches sufficient to support wildlife, the algorithm is equally well suited to defining ecologically relevant canopy openings within a forested area (Lydersen et al. 2013, Fry et al. 2014, Ng et al. 2020). The key parameters of PatchMorph are the gap threshold (gapThresh) and spur threshold (spurThresh). We set gapThresh to 12 m and spurThresh to 10 m for this analysis.

The resulting ICO distribution datasets were used to statistically compare the stand structure of the forest at the end of the frequent fire period (1941); at the end of the fire exclusion period (1995 at IS, 2006 at OH); and in modern times, after 1–2 fires had returned (2018).

We used Fisher's exact test to compare the number of tree clumps observed for each clump size between the three reference years (from 1–15 trees per clump at IS; 1–18 at OH), providing an estimate of the degree of overall forest composition change at each site. To find changes specific to individuals and binned clump sizes, contingency analysis of binned structural categories was performed, aggregating both IS and OH and using Fisher's exact test with a Bonferroni correction due to multiple tests (significance threshold of $p < 0.0125$). Bins included singletons (1-tree clumps), and small (2–4 trees), medium (5–9), and large (10+) clumps (Lydersen et al. 2013, Churchill et al. 2017). We compared the distribution of binned forest openings and binned clumps at both sites in all three reference years using permutational multivariate analysis of variance (PERMANOVA), with "Plot" as a blocking variable due to repeated measures. Gap-size bins were 82–500, 500–1500, 1500–2500, and > 2500 m^2. Data manipulation and statistical analyses were performed in R (4.2.2) using the dplR, patchwork, spatstat (Baddeley et al. 2024), sf (Pebesma et al. 2024), terra (Hijmans et al. 2024), and vegan (Oksanen et al. 2024) packages.

3. Results

3.1 Non-spatial forest structure metrics

Variable	Units	Description
TPH	trees ha^{-1}	Density of stems per hectare
SDI	–	Stand density index
QMD	cm	Quadratic mean diameter
mean DBH	cm	Arithmetic mean diameter
BA	m^2 ha^{-1}	Total basal area of stems per hectare

Table 1.1: *non-spatial metrics of forest density and tree size.*

Our analyses of non-spatial forest metrics (Fig. 1.1) showed no evidence for a change in average live tree DBH between 1941 and the fire-excluded reference year (IS, p = 0.32, 0.89; OH, p = 0.17, 1), a period of 54–65 years. The number of trees per hectare (TPH) across both sites increased significantly in the same period (+61.8 trees [25.0 per acre], 95% CI 8.5–115.1, p = 0.03). Basal area (BA) across both sites increased significantly (+10.7 m^2 ha^{-1} [46.6 sq ft per acre], 95% CI 6.9–11.9, p = 0.0003). Stand density index (SDI) increased significantly from 73.9 to 141.5 (p < 0.001).

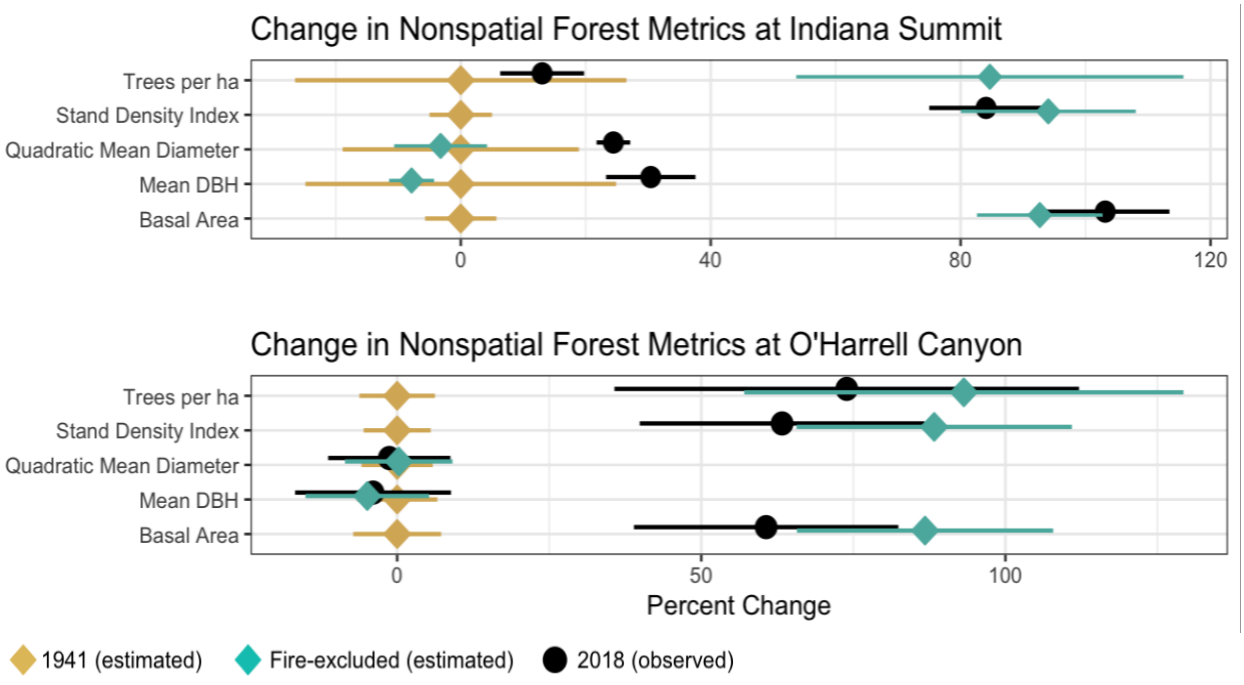

Fig. 1.1: *Change in non-spatial forest metrics at Indiana Summit and O'Harrell Canyon. 1941, the frequent-fire reference year, represents the baseline, with fire-excluded and modern conditions shown as percent change.*

We made similar comparisons between metrics for the fire-excluded forest and the modern forest. Over this 12–23-year period, average live tree DBH increased significantly at IS (+13.8 cm [5.4 in], 95% CI 9.9–17.7; $p << .001$), while at OH it did not change ($p=0.39$). IS also exhibited a marginally significant increase in QMD for this period (treated as a plot-level variable, $p = 0.05$). The change in TPH across both sites was negative but not significantly so ($p = 0.13$). Basal area did not change significantly ($p = 0.77$) and was the only metric that showed opposite signs at either site for this time period (slight increase at IS, decrease at OH). SDI decreased, but not significantly (141.5 to 129.1; $p = 0.46$).

3.2 Stand maps

The clump detection algorithm allowed a comparison of individuals, clumps, and openings at each site and across both sites during the fire exclusion period (Fig. 1.2a and b). At IS, average clump size increased from 1.45 to 2.53 trees, an increase of 1.08 trees ($p << .001$). At OH, average clump size increased from 1.29 to 1.96 trees, an increase of 0.67 trees ($p << .001$). Across both sites, the average clump size increased from 1.38 to 2.26 trees (+0.88, $p << .001$).

The proportional area belonging to each structural category shows a shift toward larger clump sizes, and away from single trees and openings, for each site during the fire exclusion period (Fig. 1.3). At each site, the most notable change in structural categories on a per area basis was the decreased area in openings (-18.2% at IS, -24.9% at OH).

From the end of the fire exclusion period to the modern forest, average clump size did not change significantly at either site (IS, $p = 0.48$; OH, $p = 0.79$), nor for both sites pooled together ($p = 0.36$). The proportion of plot area in forest openings increased by 10.7% at IS and 9.3% at OH during this period.

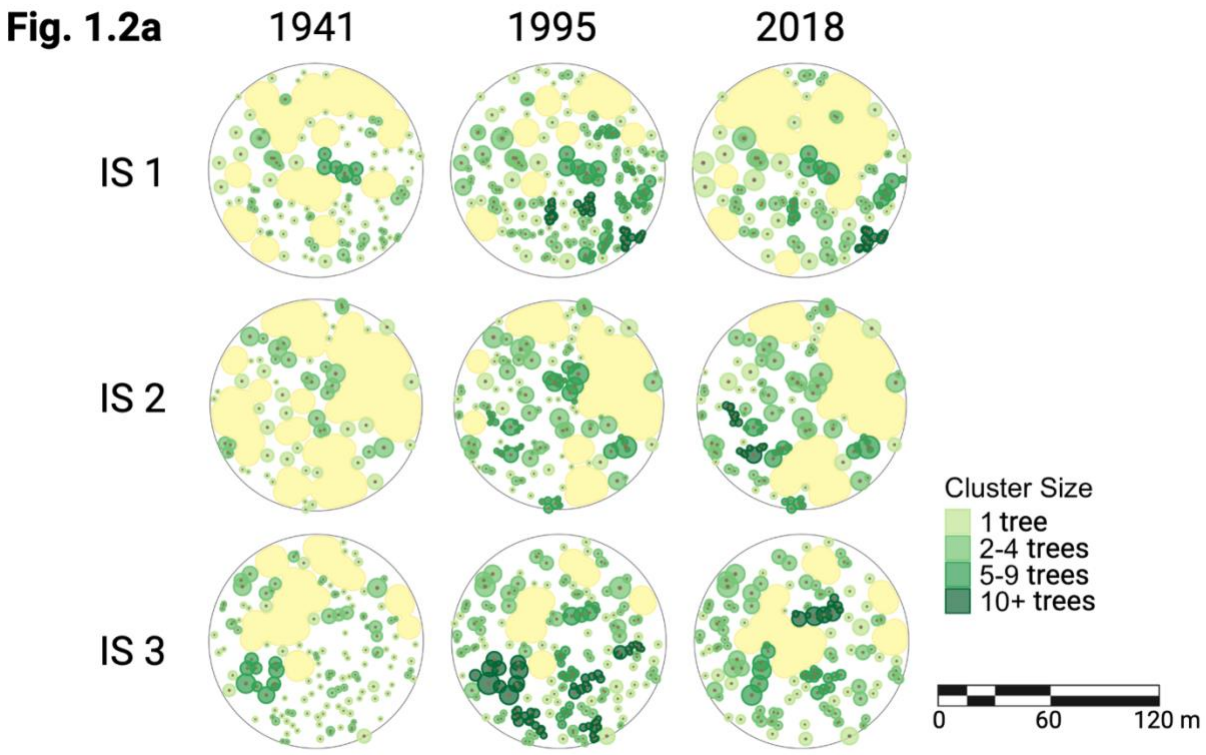

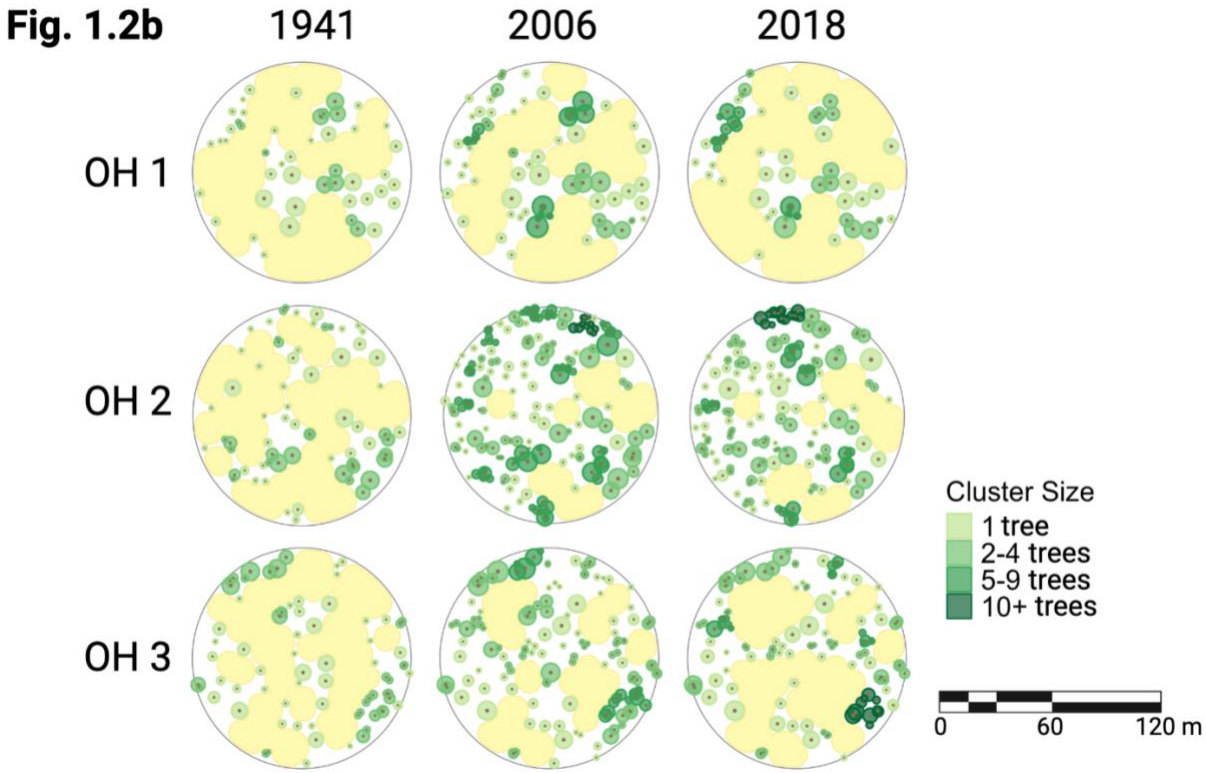

Fig. 1.2: *Top-down maps showing crowns and stems of living trees at Indiana Summit (1.2a) and O'Harrell Canyon (1.2b). Columns show frequent-fire reference year (1941, reconstructed); fire-excluded reference year (1995 at IS and 2006 at OH, reconstructed); and the modern reference year (2018, observed). Each plot (rows) is 1 ha in size.*

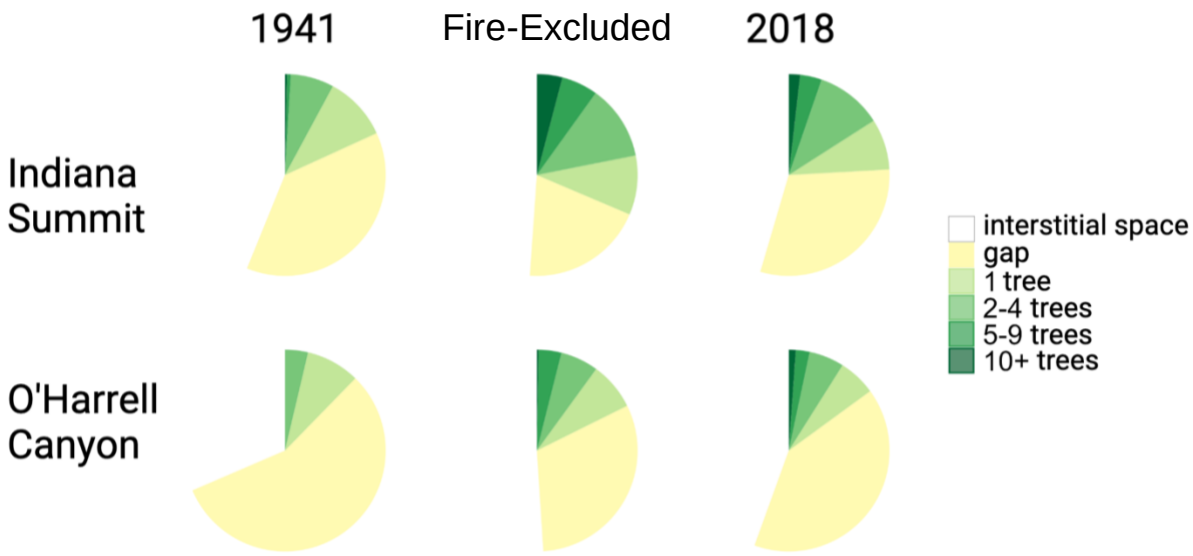

Fig. 1.3: *Proportion of forest area in each structural group: individuals; small (2-4 tree), medium (5-9 tree), and large (10+ tree) clumps; and interstitial space. At each of the two sites (Indiana Summit, top row; O'Harrell Canyon, bottom row) we surveyed three 1-ha plots, which have been aggregated for this analysis. Columns show the frequent-fire reference year (1941, reconstructed); the fire-excluded reference year, one year before the return of fire (1995 at IS and 2006 at OH, reconstrcuted); and the modern reference year (2018, observed).*

3.3 Changes in distribution of Individuals, Clumps, and Openings

The change in the overall frequency distribution of singletons and tree clumps of all sizes was highly significant at both sites from 1941 to the fire-excluded reference years ($p < 0.001$ at IS, $p = 0.03$ at OH), but not from the fire-excluded years to 2018 ($p = 0.94$, 0.92) (Table 1.2). Binned forest openings, combined between sites, shifted towards smaller sizes in the fire-exclusion period; their distribution was marginally different between the two reference years ($p = 0.06$) (Fig. 1.4). The distribution of counts per hectare for all structural categories (binned gaps (Fig. 1.4) and binned cluster sizes (Fig. 1.5)) also changed significantly from 1941 to the fire-excluded year ($p = 0.03$).

From 1941 to the end of the fire exclusion period, the proportion of trees that were singletons decreased from 55.2–24.0% at IS, and from 62.0–34.4% at OH. Contingency analysis of binned clump sizes across both sites revealed a highly significant change in the proportions of all but one structural category from 1941 to the end of fire exclusion: a decrease in the proportion of tree clumps that were singletons (76.5 to 58.3%, $p << .001$); an increase in small (2–4 tree) clumps that did not meet the

		IS in 1941	IS Fire-Excluded	IS in 2018	OH in 1941	OH Fire-Excluded	OH in 2018	All in 1941	All Fire-Excluded	All in 2018
Singletons	# Singles/ha	45.3 (19.1)	36 (7.5)	22.7 (6.7)	34 (2)	38.7 (5)	33.7 (10.4)	39.7 (13.7)	37.3 (5.9)	28.2 (9.9)
	Proportion of trees (%)	55.2 (4.5)	24 (3.6)	24.5 (6)	62 (9.8)	37.5 (12.9)	34.4 (5.1)	58.6 (7.8)	30.8 (11.2)	29.4 (7.4)
	Mean DBH	27 (12.4)	28.7 (2.6)	46.5 (8.9)	36.9 (5.7)	33.1 (10.7)	42.7 (10.9)	32 (10.2)	30.9 (7.4)	44.6 (9.2)
	BA (sq m/ha)	3.7 (1.6)	3.3 (1.6)	5.6 (3.6)	6.3 (1.2)	6 (2.7)	7.3 (0.6)	5 (1.9)	4.6 (2.5)	6.4 (2.5)
	Proportion of plot area (%)	10.3 (1.2)	9.5 (3.1)	8.2 (3.9)	8.6 (1.7)	7.7 (2.6)	6 (2.8)	9.5 (1.6)	8.6 (2.7)	7.1 (3.2)
Small Clusters (2-4)	# Clusters/ha	15 (7)	22.3 (6.4)	17.7 (3.1)	8.7 (2.3)	16.3 (9)	15.7 (9.6)	11.8 (5.8)	19.3 (7.7)	16.7 (6.5)
	Proportion of trees (%)	40.3 (0.9)	38.8 (1.6)	45.6 (4.9)	38 (9.8)	34.6 (14.3)	38.1 (8)	39.1 (6.3)	36.7 (9.4)	41.8 (7.2)
	Mean DBH	42.8 (24.6)	38.9 (9)	51.5 (6.2)	48.2 (7.8)	44.1 (7.6)	42.9 (15.2)	45.5 (16.6)	41.5 (8)	47.2 (11.4)
	BA (sq m/ha)	7 (2.4)	11.8 (1.6)	13.6 (3)	5.2 (1.4)	9.1 (3.9)	7.2 (3.2)	6.1 (2)	10.4 (3)	10.4 (4.5)
	Stem density/ha	577.1 (135.9)	626 (70.6)	536.1 (123.5)	743.5 (177.3)	896.4 (270.8)	805.6 (116.1)	660.3 (168.1)	761.2 (230.8)	670.9 (182.4)
	Proportion of plot area (%)	7 (1.8)	12 (4)	10.7 (3.5)	3.7 (2.4)	6.1 (4.6)	5.6 (3)	5.3 (2.6)	9 (5)	8.2 (4)
Medium Clusters (5-9)	# Clusters/ha	0.3 (0.6)	6 (1.7)	3.3 (0.6)	0 (0)	5.7 (4.6)	3.7 (1.2)	0.2 (0.4)	5.8 (3.1)	3.5 (0.8)
	Proportion of trees (%)	2.1 (3.7)	22.3 (10.5)	17.3 (2.8)	0 (0)	25.4 (12.8)	21.3 (9.5)	1.1 (2.6)	23.8 (10.6)	19.3 (6.7)
	Mean DBH	63.4 (NA)	33.4 (3.2)	49.7 (10.4)	-	43.4 (9.7)	34.2 (8)	63.4 (NA)	38.4 (8.4)	42 (11.9)
	BA (sq m/ha)	0.9 (1.5)	6.4 (2.9)	5.7 (0.7)	0 (0)	7.4 (3.7)	3.4 (2.3)	0.4 (1)	6.9 (3)	4.6 (2)
	Stem density/ha	35.9 (62.1)	373.2 (212.3)	212.5 (92.8)	0 (0)	865.6 (623.1)	503.5 (362.7)	17.9 (43.9)	619.4 (496.1)	358 (285.4)
	Proportion of plot area (%)	0.6 (1)	5.8 (2.1)	3.5 (1.3)	0 (0)	3.7 (2.4)	2.2 (0.5)	0.3 (0.7)	4.7 (2.3)	2.8 (1.1)
Large Clusters (10+)	# Clusters/ha	0.3 (0.6)	2.7 (2.5)	1.3 (0.6)	0 (0)	0.3 (0.6)	0.7 (0.6)	0.2 (0.4)	1.5 (2.1)	1 (0.6)
	Proportion of trees (%)	2.4 (4.2)	14.9 (13.8)	12.6 (5.5)	0 (0)	2.5 (4.4)	6.2 (5.4)	1.2 (3)	8.7 (11.4)	9.4 (6)
	Mean DBH	70.4 (NA)	28.9 (10.7)	35.3 (15.1)	-	15.9 (NA)	45.7 (11.6)	70.4 (NA)	24.5 (10.7)	39.4 (13.4)
	BA (sq m/ha)	1.4 (2.5)	3.8 (5.3)	1.8 (1)	0 (0)	0.1 (0.2)	1.7 (1.5)	0.7 (1.8)	2 (3.9)	1.7 (1.1)
	Stem density/ha	37.1 (64.3)	222.9 (199.4)	162.8 (112.3)	0 (0)	77.2 (133.6)	116.6 (105.4)	18.6 (45.5)	150 (171.5)	139.7 (100.6)
	Proportion of plot area (%)	0.4 (0.6)	4.1 (4.1)	1.8 (0.3)	0 (0)	0.3 (0.5)	1.1 (1.2)	0.2 (0.4)	2.2 (3.3)	1.5 (0.9)
Stand	Stem density/ha	101.7 (40.5)	188.3 (4.2)	120 (10.5)	62.7 (13.3)	130.7 (54)	112.3 (49.1)	82.2 (34.4)	159.5 (54.9)	116.2 (32)
	BA (sq m/ha)	12.9 (1.6)	25.3 (1.6)	26.8 (1.4)	11.5 (0.6)	22.6 (5)	19.6 (5.1)	12.2 (1.3)	24 (3.6)	23.2 (5.2)
	Mean DBH	35.5 (15.1)	34 (3)	47.4 (2.8)	41 (4.8)	38.5 (6.7)	40.7 (7.4)	38.2 (10.5)	36.3 (5.3)	44 (6.2)
	Mean trees/cluster	1.4 (0)	2.5 (0.2)	2.4 (0.4)	1.3 (0.1)	1.9 (0.5)	1.9 (0.1)	1.4 (0.1)	2.2 (0.5)	2.1 (0.4)
	Max trees/cluster	7 (3)	12.3 (3.8)	11.7 (1.5)	3.3 (0.6)	9.3 (4.2)	11.3 (4.2)	5.2 (2.8)	10.8 (3.9)	11.5 (2.8)
	Mean gaps/ha	6 (2)	5.7 (1.5)	3.7 (0.6)	2.7 (1.5)	4.7 (1.2)	3.3 (2.1)	4.3 (2.4)	5.2 (1.3)	3.5 (1.4)

Table 1.2: *Summary of characteristics, across sites and years, of individual trees; small, medium, and large clumps of trees; and stand-level structure. Figures are mean and (standard deviation).*

threshold for statistical significance (22.8 to 33.9%, p = 0.29); an increase in medium (5–9 tree) clumps (0.3 to 9.1%, p << .001); and an increase in large (10+ tree) clumps (0.3 to 2.3%, p << .001).

While there was a shift toward less total area in openings during the fire-exclusion period, the average number of openings per hectare increased (from 4.3 to 5.2). The average gap size across both sites decreased by over half (from 1086 m^2 to 493 m^2), although this change was only marginally statistically significant (p = 0.07).

From the end of the fire-exclusion period until 2018, none of the clump sizes showed a significant change. The average openings per hectare decreased from 5.2 to 3.5, though not achieving statistical significance (p = 0.13). The overall change in the distribution of binned forest openings was not significant (p = 0.31), but the distribution of counts per hectare for all structural categories was marginally significant for this period (p = 0.06). However, the average gap size in 2018 was 1014 m^2, and mean gap size was not significantly different from mean gap size in the original 1941 forest (p = 0.87).

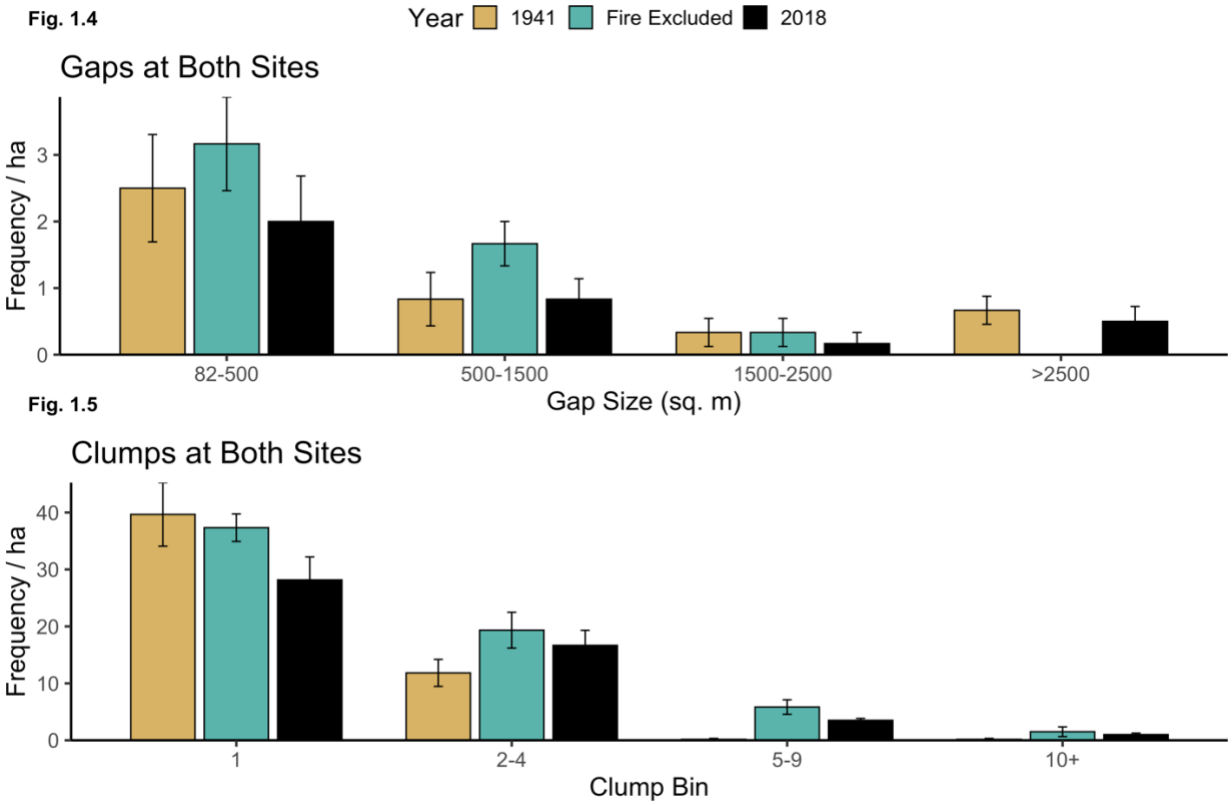

*Frequency distribution of forest opening size categories, expressed in square meters (**Fig. 1.4**) and tree clump size categories, in number of trees per clump (**Fig. 1.5**), averaged across Indiana Summit and O'Harrell Canyon. Bars represent standard error.*

4. Discussion

4.1 Overview

Our results showed that 54–65 years of fire exclusion in an Eastern Sierra Jeffrey pine forest led to denser stands with fewer, smaller openings and larger clumps of trees. The changes observed were aligned with trends in more mesic Western Sierra mixed conifer forests, with two exceptions: (1) average DBH did not decrease in our study system, as it has across much of the Western Sierra in fire-excluded stands; (2) the fire-excluded forest in our study had much lower average cluster size than fire-excluded West-side forests. Comparing the fire-excluded forests to the 2018 condition, after 1–2 fires, we found that the return of fire to the landscape had partially reversed the changes that occurred during the fire exclusion era.

4.2 Frequent-Fire to Fire-Excluded Period (1941 to 1995/2006)

Increases in average clump size, more area in large clumps, and less area in gaps is consistent with changes observed in fire-excluded Western Sierra forests (Lydersen et al. 2013) and with comparisons to a different old-growth Jeffrey pine forest in Northern Mexico (Fry et al. 2014); however, our site had about twice the proportion of single trees as these Western Sierran and Northern Mexican analogues, and only one-fifth to one-third as many trees in large clumps. (We compared our Fire-Exclusion dataset with Lydersen et al.'s 1929 and Fry et al.'s Northern Mexico sites, because the fire exclusion period for each was 40 and 68 years, comparable to our 54–65.) The change in average gap size and gap size distribution was pronounced during the period of fire exclusion, but it was neither the most nor the least extreme result among studies on Western forest reference conditions. On the West slope of the Sierra, the era of fire suppression all but erased forest openings from the landscape in many areas (although typically this change took two to three times longer than the half-century of fire exclusion experienced at our sites) (Lydersen et al. 2013). By contrast, Fry et al. found no significant difference in gap size distribution between fire-adapted *P. jeffreyi* forests in Northern Mexico and their fire-suppressed Sierra comparison sites. Although we observed an increased density of stems and increased average clump size during the fire-exclusion period, a slower rate of growth, dry conditions, and predominance of

shade-intolerant species mean eastern Sierra forests are less departed from frequent-fire conditions than their west-side counterparts. The consistent average DBH may also be in part due to the lack of logging activity in our study area, which tends to remove the largest trees. Our findings for this period were in agreement across both our study sites (IS and OH).

As on the western side of the Sierra, a lack of fire led to a change in species composition, at least at one of our two sites. While IS was nearly a pure *P. jeffreyi* stand in all three reference years (with single-digit numbers of *P. concolor* the only exception), OH exhibited more species diversity, and a shift towards more shade-tolerant species during the fire exclusion period. In the 1941 forest reconstruction for OH, we found that *P. jeffreyi* made up 86.1% of the live trees, with only 3.1% *A. concolor* and 10.6% *J. grandis*. The fire-excluded condition there (2006) featured 63.8% *P. jeffreyi* in the live-tree canopy, with 11.2% *A. concolor* and 20.7% *J. grandis* (the remainder *P. concolor*). This finding is consistent with observations across Western U.S. forest, that fire-suppressed forests feature higher proportions of shade-tolerant trees like *A. concolor* compared to frequent fire forests (McIntyre et al. 2015, Safford and Stevens 2017).

4.3 Fire-Excluded to Modern Period (1995/2006 to 2018)

Our results also indicate that the structural characteristics of a fire-adapted Eastern Sierra forest have been partly restored since fire returned to this landscape, especially at the site which burned twice, at moderate severity, in the last 23 years (IS). We examined the spatial and structural changes caused by the return of prescribed and/or wildfire to the landscape, by comparing the fire-excluded forest to the forest in 2018. We found that both sites recovered about half of the losses to their total area in openings (using the 1941 forest as the baseline), and average opening size was restored to 1941 levels. Average gap size and total gap area have discrete ecological impacts and are both useful metrics for restoration management.

The sites differed in the trends in their average stem density and tree size: while OH saw a modest recovery of TPH (about 20% restored to 1941 values), and had no significant change in average DBH during the fire-return period, IS, in contrast, had almost full recovery of 1941 live stem density, and an increase in mean DBH. This difference between the two sites is likely due to the fact that IS had burned

twice since the end of the fire exclusion period, and had burned more recently by the time we gathered the 2018 data (two years prior, vs. 11 years at OH). In fact, 56.2% of the increase in mean DBH at IS can be attributed to removal of the Class 1 snags (n = 181, mean DBH 21.1 cm) from the live tree population by the 2016 Clark Fire. These two cases suggest the necessity of multiple burns in restoring fire-adapted forest structure, and we caution that the severity of the fires in question is also important. Our study plots at IS were burned in a prescribed fire treatment between 1996–1998, and reburned at low-to-moderate severity in the 2016 Clark Fire. Plots *outside* the prescribed burn area from the 1996–1998 treatments burned at 37% high severity, and sustained much higher mortality. OH, which had lower stem density and fuel loads compared to IS at the time of fire' return, burned at moderate severity during its first fire event after the fire exclusion period, despite having had no prior thinning or prescribed burning. In low-density areas, and barring extreme fire weather, managed natural fire can begin the work of restoring fire-adapted stand structure. However, if dense, fire-excluded forests are exposed to high severity fire without any pre-treatment, fire is unlikely to help restore reference conditions, and may instead cause high enough mortality to put large areas of the forest at risk of regeneration failure (Meyer et al. 2019).

4.4 Limitations

The methods of our study feature a number of limitations which may affect the interpretation of our results. A key assumption of our study is that the frequent fire period lasted until the mid-20th Century at both sites. We base that assumption on a study of fire scar data from the forests surrounding our two study sites (North et al. 2009), but did not conduct original research for the purpose of developing site-specific fire histories. One team conducting research at Site 395, close to our sites, concluded (first) that fire cessation began in 1892 in this area, as in other Sierra sites; and (second) that the Jeffrey pine forests of the area experienced a 170-year gap in recruitment from the mid-18th to early 20th Century (Brown et al. 2010). The latter finding is in conflict with our own results, which do not support the occurrence of a recruitment gap at that time, and we propose that the lack of evidence of fire scarring was related to low sample size.

Our choice of study site was partly motivated by the relatively late start of fire suppression in the area, but it is difficult to attribute that sustained fire period to either the circumstances of land use history or local climate alone. Fire suppression started later here at least in part because European colonizers used the area primarily for mining rather than farming or grazing (North et al. 2009), and did not establish large permanent populations. The high elevation, harsh winters, and poor soil contribute both to the growth conditions in the area and the type of land use by indigenous people and settler-colonizers.

There are certain disadvantages to choosing presettlement conditions as a reference condition for fire-adapted forests, or any type of ecological restoration: some consider it overly prescriptive, as climate and society have changed dramatically (Urgenson et al. 2018); and past conditions may have exhibited nonequilibrium dynamics, making them less useful as management targets (Swetnam et al. 1999). Still, spatially explicit reference conditions are the best-suited to testing against projected climate conditions (Churchill et al. 2013).

Over the course of the 77 years examined in our study, the slow changes brought about by fire exclusion were occurring in tandem with, and likely influenced by, changes in global climate. Atmospheric CO_2 levels have risen by about 100 ppm since then (Gulev et al. 2021), hastening both abrupt disturbances like hotter droughts, and also gradual shifts in growing conditions (USGCRP 2018). Forest mortality in Sierra Nevada increased twofold 1983-2004 (van Mantgem and Stephenson 2007), and forests in the southwestern United States have a demonstrated lack of regeneration due to climate-related changes in environmental stresses like soil water and temperature (Petrie et al. 2023). It is likely that during the fire exclusion period (1941-1995/2006), the increased stand density indicated in our results occurred in *spite* of climate-induced increases in mortality rates. On the other hand, the effect of fires from 1995-2018, restoring lower-density forests with more openings, was probably aided to some degree by climate-induced increases in mortality and reductions in regeneration.

4.5 Conclusions and Management Recommendations

Our study provides the first spatially explicit evidence of fire suppression and fire return's effects on Eastern Sierra Jeffrey pine forests, which can inform management decisions in this ecosystem.

In seeking to restore frequent-fire conditions, forest managers have a number of tools at their disposal: Western Sierra studies on fuels management focus on mechanical treatments, prescribed fire, and their combination, with an additional variable to account for the frequency of application for each treatment (Stephens et al. 2024, Brodie et al. 2024). Such research has found that a combination of thinning and prescribed burning is typically the most effective in moderating the effects of modeled (Stephens et al. 2024) and real-world (Brodie et al. 2024) fire return. The longevity of treatment effects depends on site productivity, indicating that such treatments can have long-lasting effects in dry, relatively slow-growing East Sierra Jeffrey pine forests.

The Eastern Sierra Climate and Communities Resilience Project, informally known as the "Mammoth Donut," is an ambitious project that will unfold over the next 15-20 years, attempting to return the forests to a condition that can withstand both prescribed and managed natural fire (Pusina et al. 2023). As the Clark Fire at IS demonstrated, high-severity, uncontrolled wildfire can have devastating impacts on fire-suppressed forests if they have not been treated with some level of active management in preparation (Meyer et al. 2019). Our study shows that first- and second-entry, low-to-moderate-severity fires (natural at OH, and a mix of natural and prescribed at IS) are able to partially restore historical conditions in fire-excluded forests. Along with mastication and thinning, prescribed burns and managed natural fires will be an important tool to prepare Eastern Sierra communities for fire resistance and resilience (North et al. 2012).

Chapter 2: TinyFACE: a low-cost field experiment for elevated CO_2 research on plants

Abstract

Rising atmospheric CO_2 levels place terrestrial ecosystems under novel environmental conditions, and research in field settings is key to understanding how real plant communities will respond. Despite decades of progress in elevated CO_2 (eCO_2) experiments, major gaps persist in our knowledge of plant responses to interacting influences of climate change, especially in areas outside North America and Western Europe.

With a goal to expand access to field-based eCO_2 research, we designed, built, and tested TinyFACE, a low-cost field experiment for climate change research on plants. TinyFACE features sixteen 0.5-m^2 plot areas, half with ambient and half with elevated (+200 ppm) CO_2 concentrations.

Using a proportional-integral control algorithm and constant sampling of air within the plots, TinyFACE achieves consistent elevation averaging +196.9 ppm. During testing, 95.1% of measured CO_2 concentrations fell within 20% of the set point (ambient CO_2 + 200 ppm). A streamlined design and efficient use of instrumentation reduced the cost of the system to as low as one-fourth of the cost of similar experiments from the past 30 years ($16.57 vs. $64.65 ppm^{-1} m^{-2}, adjusted to 2024 USD).

Our results demonstrate a system capable of precise and accurate field-based CO_2 elevation for significantly reduced cost. We envision the TinyFACE design being implemented in a multitude of field-based eCO_2 studies, perhaps as part of a globally distributed collaborative network experiment.

Keywords: climate change research, CO_2, experimental ecology, FACE, plant physiology

1. Introduction

Atmospheric CO_2 concentrations are at their highest level in 3 million years (Gulev et al. 2021), and while they are projected to continue rising, they have already dramatically changed Earth's biosphere. To study plant responses to rising CO_2 levels, researchers have long been interested in exposing field-grown plants to CO_2-enriched (eCO_2) air, thus avoiding the pot and chamber effects and altered

microclimates of enclosed planting areas (Ainsworth and Long 2021), and solving the problem of low correspondence between field-grown and lab-grown plants (Poorter et al. 2016). The most prominent example of this type of study is Free-Air CO_2 Enrichment (FACE). Field-based eCO_2 research methods like FACE are not new: the first FACE studies began more than 35 years ago (U.S. DOE 2020), comparing plant growth at ambient CO_2 levels (then, 360 ppm) and under eCO_2 treatment (550 ppm). Mean annual CO_2 levels today have surpassed 420 ppm (Gulev et al. 2021). At current emissions levels, they will reach 550 ppm within a few decades (IPCC 2021), meaning that in field settings, what once passed for CO_2 treatment will become the control. The accelerating increase in global CO_2 concentrations, and the myriad questions still left to explore using field-based eCO_2 experiments, motivated us to design a system that will make these methods more accessible for climate change researchers.

Although three decades have passed since the first FACE studies began, the spatial bias in this type of research has been largely unchanged, with the large majority of studies occurring in temperate ecosystems, mainly in North America and Europe (Norby et al. 2016). As recently as 2014, of 147 studies reviewed, over 75% were in temperate forests (68%) or grasslands (8%) (Jones et al. 2014). Few FACE studies have occurred in boreal and tropical ecosystems, in spite of those ecosystems' high capacity for carbon storage and uptake—one tropical rainforest FACE system (AmazonFACE) and one boreal FACE system (SwedFACE), begun in 2016 and 2017 respectively, are the only exceptions thus far (Norby et al. 2016). Rather than maintaining or even accelerating the addition of FACE studies to rectify this imbalance, interest in funding FACE and similar studies has dwindled since the late 2010s, leading to a decline in field-based eCO_2 research (Jones et al. 2014, Fangmeier et al. 2016, U.S. DOE 2020). Expanding access to eCO_2 research methods will therefore require minimizing costs while maintaining the rigorous standards of the FACE research protocol.

Since the late 1990s, FACE researchers have applied certain standards for spatial and temporal control: namely, less than 10% deviation in mean CO_2 concentration between the center of a treatment plot and any other point within the plot; and at least 80% of measured CO_2 concentrations falling within 20% of the eCO_2 set point (Miglietta et al. 2001). In addition to these standards, FACE and other eCO_2

studies typically seek to avoid creating microclimate effects that alter the plant growth environment in unintended ways. eCO_2 studies have taken various approaches to simultaneously minimize costs, maximize design flexibility and number of replicates, ensure homogeneous CO_2 distribution, and avoid microclimate effects (Fangmeier et al. 2016). Study designs include full-scale FACE experiments (up to 3000 m^2 in size) (U.S. DOE 2020), miniature FACE experiments (Miglietta et al. 2001), open-topped chambers (OTCs) (Messerli et al. 2015), and systems to distribute CO_2 directly into the plant canopy through porous tubes (Pepin and Körner 2002, Fangmeier et al. 2016), among others. We chose Screen Aided CO_2 Control (SACC), a middle ground between traditional FACE and OTCs, which is appropriate to short-stature plants (up to 0.5 m in height).

SACC is less expensive than true miniature FACE due to lower CO_2 supply, but it avoids most of the undesirable microclimate effects of OTCs (Leadley et al. 1997). For instance, the first example of a SACC system featured a near-surface air temperature difference of +1ºC over the control as an artifact of the system design, compared to +1–3ºC for contemporary OTCs. Additionally, peak air temperatures within SACC units did not exceed +2.5ºC above controls, while OTCs were found to cause +4–7ºC change in peak temperatures (Leadley et al. 1997). Lower cost per treated area provides the opportunity for larger plots, more replicates, higher CO_2 treatment levels, or a combination of all three. More replicates and larger plots can provide space for multi-factor experiments, with (e.g.) water stress, temperature, ozone or other pollutants as a secondary treatment, allowing tests for interactions between multiple ecophysiological variables (Way et al. 2015). Alternatively, even single-factor, moderately replicated FACE studies would be novel and useful in the many tropical and boreal ecosystems that are still understudied in the history of eCO_2 research (Jones et al. 2014).

Our goal in this study was to design, test, and describe a new SACC system for eCO_2 research on plants in field settings, hereafter called TinyFACE. TinyFACE is capable of CO_2 enrichment consistent with other published eCO_2 studies of short-stature plants, at as low as one-third of the cost. We describe the design, construction, and performance of the TinyFACE system, and discuss potential applications of the system in future climate change research.

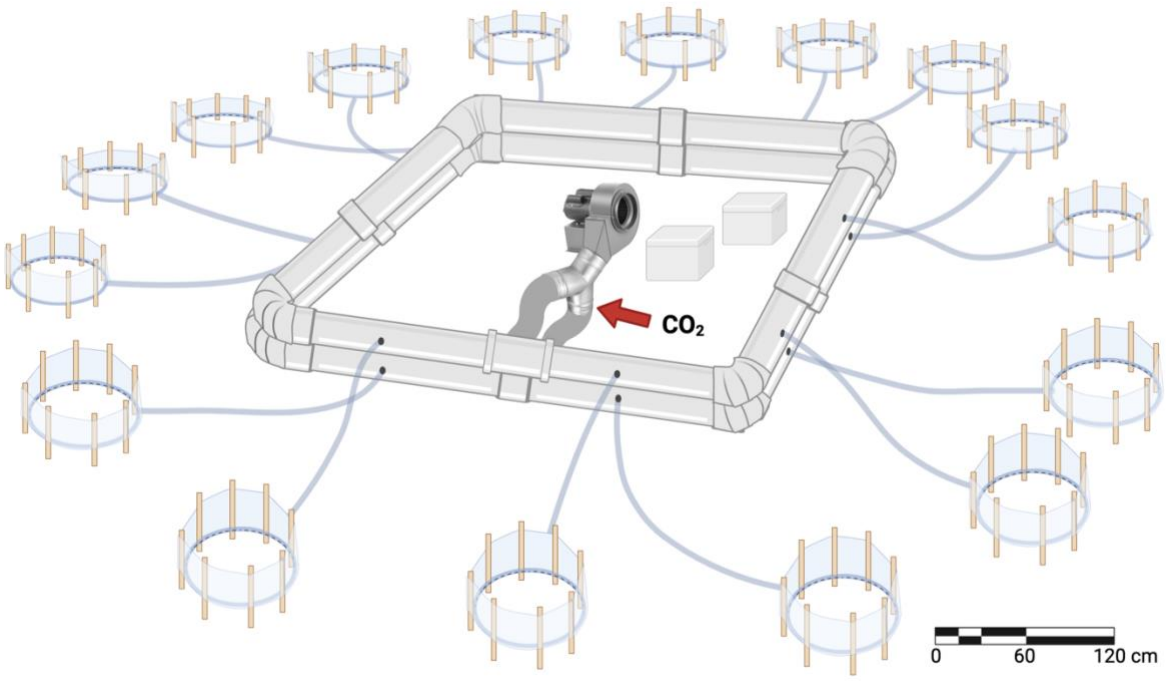

Fig. 2.1: *Structure and layout of TinyFACE, a field-based system for performing CO_2 enrichment experiments in plants. Shown are the central blower, the ducting system and outlet tubes for air delivery, and the sixteen 0.5-m^2 growth plots, which house study organisms (not pictured). The red arrow indicates the point of CO_2 injection into the lower level of the ducting system.*

2. Materials and Methods

TinyFACE (Fig. 2.1) is a modular, customizable CO_2 enrichment system, designed for growing small plants in field settings under the conditions of future climates. The version described here, constructed in January 2022, includes sixteen circular 0.5-m^2 plots, with half of the plots receiving eCO_2, and half serving as ambient controls. The CO_2 enrichment system itself is composed of two subcomponents, one for CO_2 injection and bulk air flow (Air Supply) and the other for CO_2 regulation and data collection (Measurement). CO_2 injection is regulated by an algorithm that responds to per-minute plot-level CO_2 data collected by the measurement system.

2.1 Site Description

The TinyFACE system was built, tested, and operated at Quail Ridge Reserve of the University of California Natural Reserve System, in Napa County, CA. The experimental site is next to the Researcher House, on the eastern side of the ridge, at 365 m elevation. The area occupied by TinyFACE has a slight slope of 1.7º, with an aspect of 88º. Average precipitation at the site since 2017 is 44.8 cm per

year, falling mainly between the months of October and March. The open blue oak (*Quercus douglasii*) woodland at this location is sheltered by surrounding hillsides, and thus protected from extreme high winds. Average temperatures are 8ºC in January and 28ºC in July (UC NRS 2015).

2.2 Air Supply System

CO_2 delivery is achieved through two closed circuits of 8" (20.3 cm) snap-lock galvanized steel ducting (Fig. 2.1). The ambient CO_2 circuit is stacked on top of the elevated CO_2 circuit, supported by 1.2 m wooden stakes, and together they form a 3.8 × 3.5 m rectangle. Each side of the rectangle has two outlet holes cut into the upper ducting, and two in the lower ducting, for a total of four outlets on each side (to fumigate 16 total plots). The holes were cut with a 32-33 mm hole saw to accommodate 3.3 cm (outer dia.) bulkhead fittings, which provided a spot for outlet tubes to attach. Two-meter lengths of flexible 3.2 cm (inner dia.) PVC tubing connect each outlet hole to a closed loop of perforated 3.2 cm PVC tubing encircling each plot. Seven mm holes drilled every 5 cm in the perforated tubes deliver air to the plots where plants are grown. The perforated pipes are mounted on 0.6 m wooden stakes, holding the pipes 10 cm from the soil surface. A semitransparent screen made of 6 mil greenhouse plastic encircles each plot from 10 to 43 cm above the soil surface. The screen allows turbulent mixing of air from the 10 cm gap at the soil surface, while slowing the dispersion of CO_2-enriched air from around the plot. The diameter of the circle encompassing each plot is 79 cm, such that each plot is approximately 0.5 m^2 in area.

In the center of the ducting system is the ⅓ horsepower, 865 cubic ft min^{-1} capacity (24494.1 L min^{-1}) blower (1963K15; McMaster-Carr, Elmhurst, IL), protected from the elements by a plywood shelter. The blower provides bulk airflow to the upper and lower ducting circuits, connected to both via a register box, a Y-shaped galvanized steel fitting, and two 1.2 m lengths of flexible aluminum ducting.

CO_2 issues from a 180L liquid CO_2 dewar (180LT350; AirGas, Radnor, PA) attached to a CGA 580 regulator. A regulator outlet setting of 0.06 MPa delivers adequate flow without over-pressurizing the system. With this setting and a CO_2 elevation level (ΔSet) of +200 ppm, one 180L dewar lasts about 45 days. UV-resistant, 0.6 cm PVC tubing (BevaLine) connects the pressurized CO_2 outlet to the CO_2

injection point in the lower branch of the ducting system, past the Y-shaped fitting at the mouth of the blower. Between the 180L dewar and the CO_2 injection point is the Mass Flow Controller (FMA5524A; Omega Engineering, Norwalk, CT), regulated by the measurement system, which dictates the volumetric flow rate of the pure CO_2 stream injected into the lower ducting system, as necessary, to achieve the desired CO_2 elevation at the plots.

2.3 CO_2 Measurement System

CO_2 control and data collection (Fig. 2.2) rely primarily on a data logger (CR3000; Campbell Scientific, Logan, UT) and a CO_2/H_2O Gas Analyzer (LI-840A; LI-COR, Inc., Lincoln, NE). The gas analyzer measures the CO_2 concentrations of air samples pumped to it from sampling points in the centers of three of the 0.5-m^2 plots. The data logger passes the CO_2 concentration data to a program containing a proportional-integral (PI) algorithm, which regulates the rate of CO_2 delivery through the Mass Flow Controller, enabling the system to respond to deviations from the desired CO_2 elevation level.

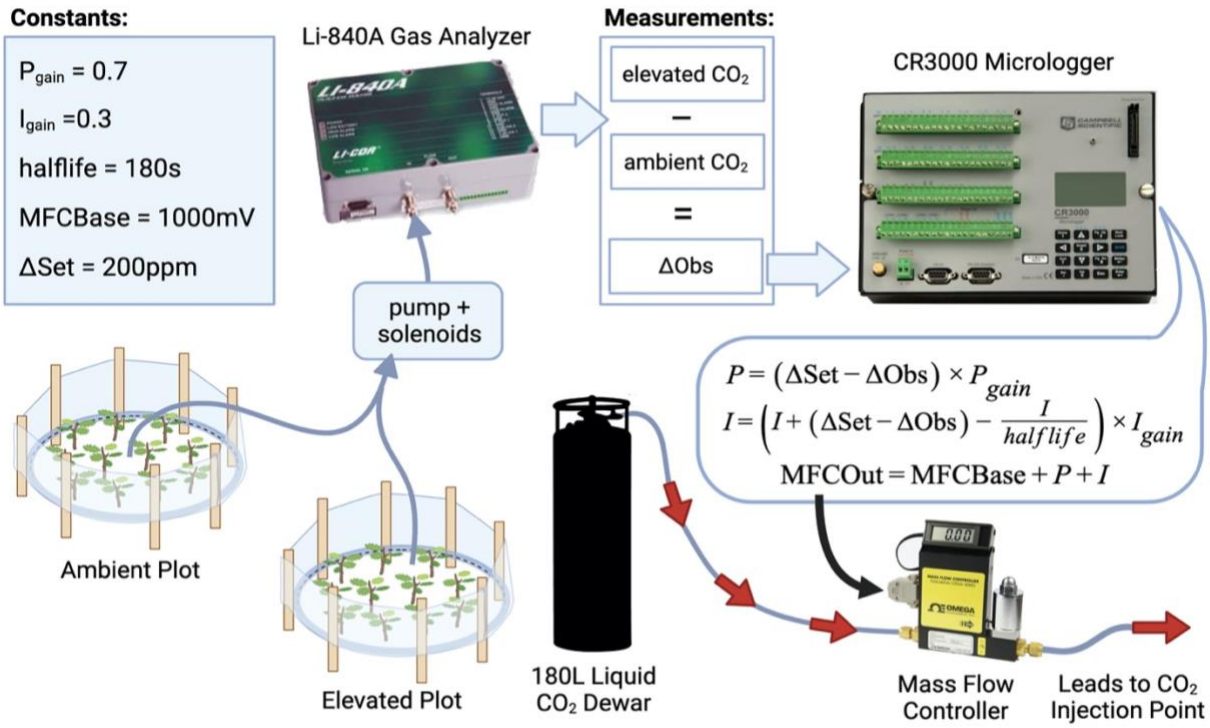

Fig. 2.2: *System control of the TinyFACE CO_2 elevation protocol. CO_2 concentrations are continuously measured in the ambient and elevated plot as shown, providing a reference for the realized elevation (ΔObs) as compared to the desired elevation (ΔSet). The difference between these numbers controls the proportional-integral algorithm (at right), which in turn up- or down-regulates the CO_2 flow via the Mass Flow Controller.*

2.3.1 PI Algorithm and CO2 Control Program

The CO_2 control program was written in Campbell Science Short Cut (v2.8) and CR Basic software, and uploaded to the data logger. The program has four main features: data collection, PI algorithm, PAR threshold for CO_2 delivery, and direct control settings (used for calibration and testing). Air samples drawn from respective plots provide the basis for Ambient CO_2 (*CO2ref*) and elevated CO_2 (*CO2elev*) measurements, which are used to calculate the observed difference in CO_2 between ambient and elevated plots (ΔObs). We chose a CO_2 treatment level (ΔSet) of +200 ppm, which is standard among FACE studies as it provides insights into expected CO_2 effects for the mid-to-late 21st Century (Ainsworth and Long 2021). When the program is running, the minute-to-minute difference between observed and desired ΔCO_2 is used to calculate the parameters of the PI algorithm:

$$P = (\Delta Set - \Delta Obs) \times P_{gain} \qquad \text{(eqn 1)},$$

where P_{gain} sets the sensitivity of the correction factor P.

$$I = I + (\Delta Set - \Delta Obs) - \frac{I}{halflife} \times I_{gain} \qquad \text{(eqn 2)},$$

where I_{gain} sets the sensitivity of the correction factor I, and *halflife* is a length of time affecting the decay rate of a given CO_2 deviation's effect on the correction factor.

$$MFCOut = MFCbase + P + I \qquad \text{(eqn 3)},$$

where *MFCbase* is a baseline number in mV that sets the Mass Flow Controller's flow to a default value capable of achieving +200 ppm; and *MFCout* is the corrected mV, accounting for P and I, that dictates the flow through the Mass Flow Controller.

Based on these equations, when ΔObs is below ΔSet, P and I take on positive values, *MFCout* is raised above the default value, and the system upregulates the CO_2 stream allowed through the Mass Flow Controller (by increasing *MFCout*). When ΔObs is above ΔSet, P and I become negative, and *MFCout* is reduced below the default value, lowering the rate of flow for the CO_2 stream passing through the Mass Flow Controller.

In our testing of the system, the best results were achieved when *Pgain* and *Igain* were set at 0.7 and 0.3, respectively; *halflife* was set at 180 s; and *MFCbase* was set at 1000 mV. (The 0–5 V setting for the Mass Flow Controller translates to a 0–20 L min^{-1} flow rate; i.e. 1000 mV corresponds to 4 L min^{-1}.) These values were determined with the use of the "MFC Direct Control" parameter, which allows the user to test different baseline settings of the Mass Flow Controller and find a suitable starting point for the PI algorithm to act upon. In summary, we calibrated a base flow of CO_2 that on average achieved the Δ*Set* of +200 ppm, and then relied on the PI algorithm to adjust for expected deviations from achieving this target.

Because our primary interest is to determine the effects of eCO_2 on photosynthesis, the data logger is programmed to shut off CO_2 delivery once ambient light levels drop below a certain threshold. The threshold value for photosynthetically active radiation (PAR) is determined by the PAR sensor, and the program specifies that at values below 50 μmol m^{-2} s^{-1} the Mass Flow Controller valve will close, preventing the flow of CO_2 to the plot during periods with insufficient light for photosynthetic activity.

2.3.2 Sampling Tubes and Instrumentation

The system control loop is based on the sampled values of *CO2ref* and *CO2elev*, which are in turn based on air samples drawn from designated ambient and elevated plots. A third sampling line (which measures *CO2test*) can be moved between various plots, or various places within and outside of the plot areas, to test for consistency in CO_2 elevation throughout the system.

Three lines of 0.6 cm BevaLine tubing connect the sampling points to the gas analyzer. Air is drawn from the plots to the gas analyzer with a 12V mini vacuum pump. To ensure regular CO_2 delivery adjustments using a single gas analyzer, the system cycles through each of the three sampling lines every minute. The cycling is achieved with the help of three solenoid valves, which receive a signal from the data logger via three ports on an eight-channel relay, and stay open for 20 s out of each minute in rotation. The average reading of each 20 s interval is stored as that line's current CO_2, and that value is then used to determine Δ*Obs* for the PI algorithm. These data are stored every 20 s. We determined that 20 s at the system's typical flow rate was enough time for air to move through the tubes from the sampling point to

the gas analyzer, by breathing into the far end of the tube and inspecting the data readout for CO_2 spikes in sampled air.

The electronic components of the CO_2 Control system (datalogger, gas analyzer, Mass Flow Controller, sealed lead acid battery, eight-channel relays, solenoid valves, power transformers, vacuum pump) are stored in two weather-proof boxes. Although in our system they were located in the same box, our recommendation is to separate the Mass Flow Controller from the gas analyzer. Otherwise, any leaks in the CO_2 injection stream through the Mass Flow Controller will affect the gas analyzer's CO_2 readings and hinder the control system's functioning.

Wind speed is measured using an anemometer 0.5 m above the soil surface. Wind speed was not associated with CO_2 control in our design, but it can be incorporated as part of the regulatory system if desired.

2.4 Budget and Parts Specifications

The structural elements of the system can be built for approximately $2500. The CO_2 supply for our preliminary study lasting 18 months (see Chapter 3) also cost approximately $2500. The instruments for monitoring and control collectively cost approximately $12,000. Table 1 contains an itemized list of components, including product names, manufacturers, and prices.

2.5 Performance Testing

The system's final calibration was performed on April 8, 2024. First, we calibrated the adjustments to readings from the gas analyzer, using the observed CO_2 concentration from (1) a canister of soda lime (0 ppm CO_2) and (2) a tank of calibration gas (297 ppm CO_2). The resulting observed "Zero" and "Span" values were used to correct the raw output from the gas analyzer and translate into ppm. Finally, we adjusted the *MFCbase* parameter to a suitable starting point (1000 mV) for achieving a CO_2 elevation of +200 ppm. Spatial and temporal control were tested on the days of April 9 and 10, 2024, and in a subsequent 10-day test from April 10–19.

During the two days of spatial control testing, we used the test sampling line to quantify performance at different points within and between the sixteen 0.5 m^2 plots. The eCO_2 sampling line

	Item Name	Model/Type/Size	Part No.	Supplier	Unit Cost	No.	Total Cost
Air Supply	Snap-lock duct	Master Flow, 8"x5'	100172984	Home Depot	$12.68	16	$202.88
	Elbow fitting	Master Flow, 8" 90º	100187427	Home Depot	$7.63	8	$61.04
	Splice collar	Master Flow, 8"	204169131	Home Depot	$16.21	6	$97.26
	Tee fitting (duct)	Master Flow, 8"	100128619	Home Depot	$18.61	2	$37.22
	Duct sealant	Master Flow Water Based	100396972	Home Depot	$4.98	2	$9.96
	Duct tape	ShurTape 2.5"x60yd	312460633	Home Depot	$16.58	2	$33.16
	Support stakes	Pine wood stakes, 1"x2"x4'	349466	Home Depot	$3.98	16	$63.68
	Bulkhead fittings	PVC, 1.3" OD	B08ZMW167T	Honoson	$4.00	20	$79.95
	Hose clamps	Everbilt 3/4-1 3/4"	202309386	Home Depot	$1.40	20	$28.00
	Flexible PVC tubing	1 1/4" ID	LPpvc125-100ft	Duda Energy	$2.43	300	$727.98
	Tee fitting (tubing)	1 1/4" x 1 1/4" OD	41776	Boshart Industries	$2.59	20	$51.80
	Screen stakes	Pine wood stakes, 1"x2"x2'	203316911	Home Depot	$0.58	180	$104.70
	Greenhouse plastic	Clear Polyethylene, 6 mil, 8'x48'	B08PNBVSKN	A&A Green Store	$69.99	1	$69.99
	Blower	120/230V AC, 865 CFM	1963K15	McMaster-Carr	$428.66	1	$428.66
	Register box	Master Flow, 14"x6" to 8"	100135879	Home Depot	$10.82	1	$10.82
	Wye	Ideal-Air Branch, 8x8x8"	736200	Ideal-Air	$37.01	1	$37.01
	Aluminum flex pipe	Master Flow, 8"x8'	204090951	Home Depot	$28.69	1	$28.69
	Bev-A-Line® IV tubing	1/8" ID x 1/4" OD x 1/16" Wall	56289	US Plastics	$0.51	50	$25.50
	Regulator	9296		Harris Products	$286.31	1	$286.31
CO2 Measurement	Data logger	CR3000 Micrologger		Campbell Science	$3,960.00	1	$3,960.00
	Gas analyzer	Li840-A CO2/H2O		LI-COR	$4,900.00	1	$4,900.00
	Mass flow controller	Max flow rate 20 L/min	FMA5524A	Omega	$1,276.26	1	$1,276.26
	PAR sensor	LI-250A		LI-COR	$279.00	1	$279.00
	LoggerNet			Campbell Scientific	$969.45	1	$969.45
	Bev-A-Line® IV tubing	1/8" ID x 1/4" OD x 1/16" Wall	56289	US Plastics	$0.51	150	$76.50
	Vacuum pump	DC 12V, 5L/min 120kpa	B08FX6VGVH	Yosoo Health	$23.00	1	$23.00
	Solenoid valves				$15.00	3	$45.00
	8-channel relay				$15.00	3	$45.00
	Battery	12V			$25.00	1	$25.00
	Weatherproof boxes				$200.00	2	$400.00
						Grand Total:	$14,523.82

Table 2.1: *parts list and budget for TinyFACE construction and operation.*

remained stationed 10 cm above the soil surface, directly over the center point of Plot 9. The test sampling line was then moved between sampling points every 20 min for the following sets of values: points above the plot center, points in a 12-point sampling grid inside the screen, points outside the screen (north, east, south, and west, in 10 cm increments from 10–50 cm), and finally the center points of each of the 16 plots. All plot-level tests were conducted on Plot 9. Lastly, taking advantage of grasses that had grown nearby, we tested CO_2 elevation performance with varying heights of vegetation: short (10 cm) grass, medium (25–35 cm), and tall (50–60 cm, above the height of the 43-cm screen); each vegetation height was measured once at canopy height and once at 10 cm above plot center.

Microclimate effects of the screens around each plot in the TinyFACE system were tested on June 29th, 2024 (daily high 31.1ºC, low 21.1ºC, cloudless). Over the course of the day (from sunup to sundown, every 2 h), we collected measurements of PAR and ground surface temperature on bare soil within the plot areas and outside the screens. For both temperature and PAR, measurements per plot were taken as the average of a 12-point sampling grid, and a subset of four plots were measured. (No difference was detected between eCO_2 and aCO_2 plots, so data were combined.) Values from outside the screens (n = 4) were taken as the average of an identical 12-point sampling grid, placed outside the enclosing screen and at least 15 cm away from the plot boundary. PAR was measured using a handheld light meter (LI-250A, LI-COR, Inc.; Lincoln, NE), comparing light received at the soil surface in vs. outside the plastic screens. Surface temperature was measured using an infrared surface thermometer (561; Fluke, Everett, WA).

Data processing and analysis was performed in R (v4.2.2). We used a gridded bilinear spline function (Akima 1978) to interpolate the data for horizontal control of CO_2 elevation at the plot level.

3. Results

Here we provide an evaluation of the system performance in terms of temporal control, single-plot and between-plot spatial consistency, and the CO_2 delivery rate required to achieve the desired elevation.

The system demonstrated consistent CO_2 elevation with good temporal control over 10+ days of testing. A density plot of observed CO_2 elevation values from Plot 9 is shown in Fig. 2.3; data are 20 s averages of daytime values between April 9–19, 2024. Over this period, mean CO_2 elevation was +196.8 ppm (sd = 63.6), and 95.1% of all elevated values were within 20% of the target concentration (ambient value + 200 ppm).

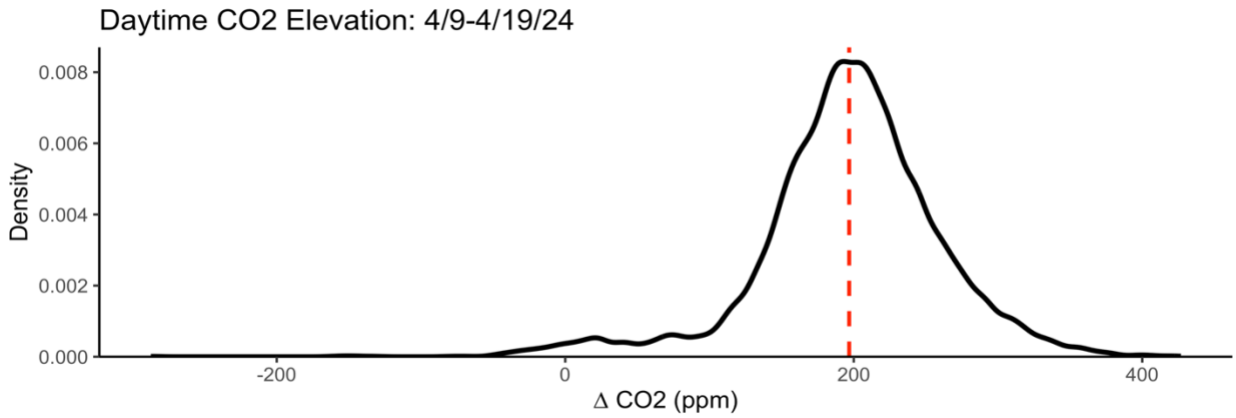

Fig. 2.3: *Density plot of CO_2 elevation over ten days of testing in April, 2024. Data represent 20 s means of the difference in daytime CO_2 concentration between ambient values and an eCO_2 treatment plot.*

Spatial control was also strong, both between the eight eCO_2 treatment plots and within the screen of a single plot. Testing between plots (conducted April 10, 2024) demonstrated an experiment-wide mean elevation of +209.9 ppm (sd = 56.7), with 100% of measurements within 20% of the target elevation, and 96.9% within 10%, during the entire between-plot testing period. Per-plot means (sd) from sampling points 10 cm above plot centers ranged from +166.4 ppm (64.6) to +238 (66.0) (Fig. 2.4).

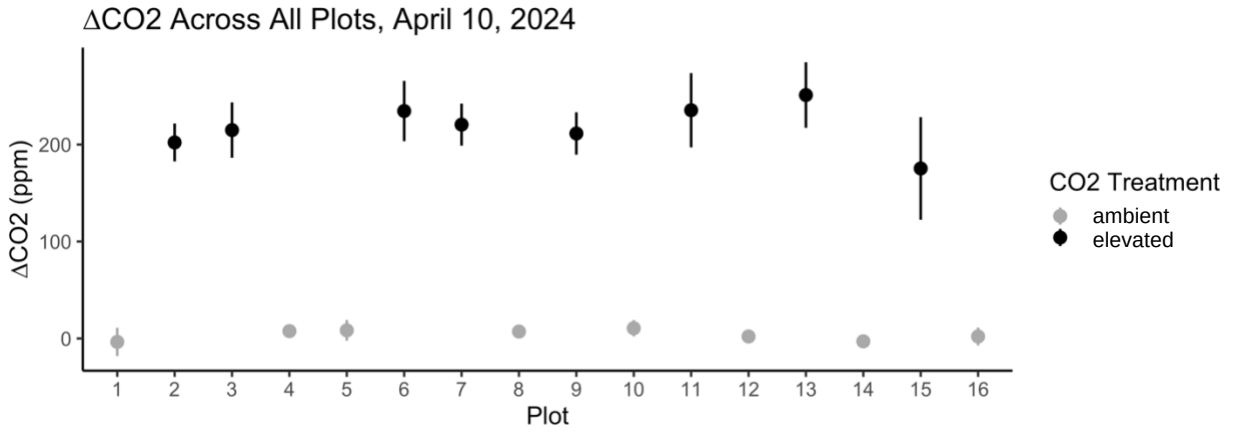

Fig. 2.4: *Mean and standard deviation of CO_2 elevation achieved for each of 16 treatment plots.*

Plot-level testing involved horizontal variation (within and outside the screen), vertical variation (above plot center), and performance with varying heights of vegetation. The average elevation across all 12 sampling points within Plot 9 was +198.9 ppm (53.4), with a range in means of 160.8–256.1 ppm. The mean difference between sampling points and the CO_2 concentration measured at plot center was -3.35% (sd = 4.35). Outside the screen, CO_2 elevation levels declined from a mean of 42.6 ppm (49.1) at 10 cm from the screen to a mean of 15.6 (36.9) ppm at 50cm. The interpolated and measured values for horizontal CO_2 control are shown in Fig. 2.5.

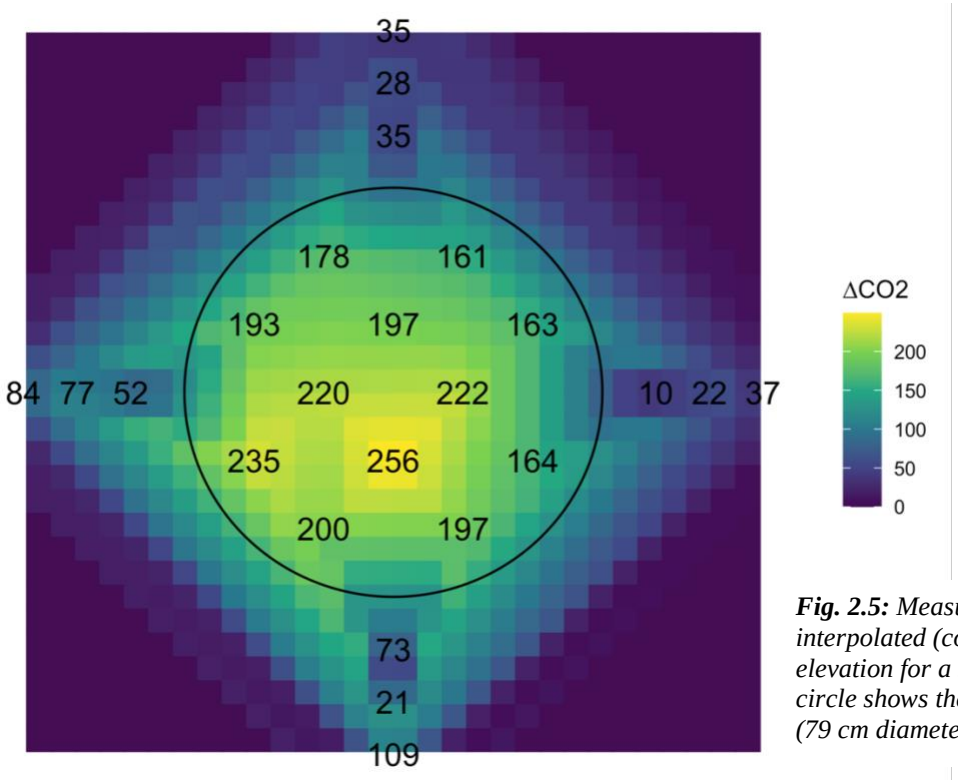

Fig. 2.5: *Measured (numbers) and interpolated (colored squares) CO_2 elevation for a single plot. The black circle shows the enclosing screen (79 cm diameter).*

Vertical control was measured in 10 cm increments directly above the plot center, from 10 cm to 100 cm in height (Fig. 2.6). Elevation values within the screen (i.e. below 43 cm in height) averaged +198.3 ppm, while values rapidly declined above the top of the screen.

We conducted limited tests on the effects of vegetation height on the CO_2 control performance of TinyFACE. CO_2 elevation sampled at 10 cm above plot center increased monotonically with vegetation height. Elevation values taken at canopy height were highest for medium vegetation and lowest for high vegetation (Fig. 2.7).

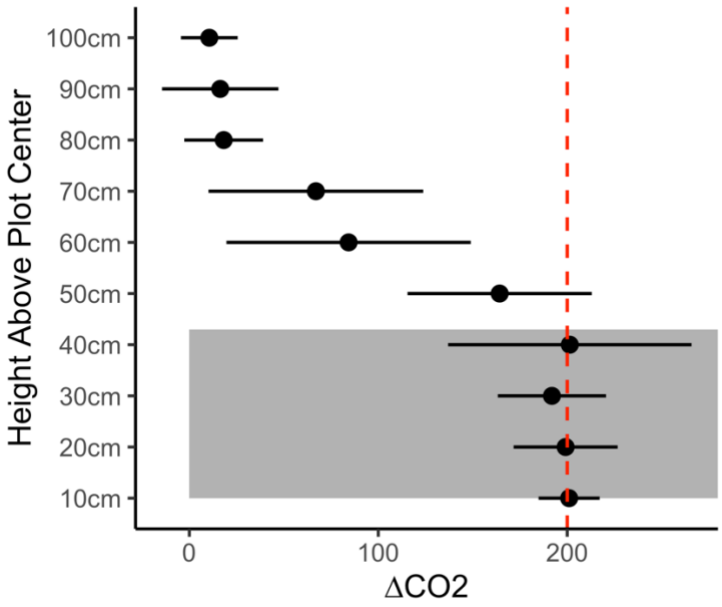

Fig. 2.6: *Mean and standard deiation of CO_2 elevation achieved at various heights above the center of a plot. In gray is shown the height of the enclosing screen, as well as the height of the gap at its base.*

During the ten-day testing period, TinyFACE demonstrated a highly efficient rate of CO_2 consumption. With an average operational flow rate of 3.97 L min^{-1} from the liquid CO_2 dewar, and a total of 4 m^2 of plot area under eCO_2 treatment, the system requires 2.62 kg CO_2 $m^{-2}d^{-1}$ when CO_2 is flowing. Because our system is designed to shut off CO_2 delivery when PAR is below 50 µmol m^{-2} s^{-1}, the 24-h average is lower, at 1.64 kg $m^{-2}d^{-1}$.

In tests on microclimate effects of the enclosing screens, we found that the screens kept the soil surface slightly cooler: the mean difference in soil temperature inside the screens averaged -2.9ºC throughout the day, compared to the mean outside the screens, with a maximum deviation of -8.3ºC at 14:00. As a percentage of average surface temperature outside the screens, these changes represented 6% and 19.2%, respectively. The screens also intercepted a fraction of solar radiation, such that PAR averaged 96.9 µmol m^{-2} s^{-1} (12%) lower within the screens throughout the day, with a maximum deviation of -217.8 µmol m^{-2} s^{-1} (28.5%) at 16:00.

Although the final calibration tests took place in April 2024, a preliminary study took place in the TinyFACE CO_2 system from Spring 2022–Fall 2023. This experiment (with different settings than those listed here) had a mean CO_2 elevation of +127 ppm above ambient values. Over the course of 18 months, 96 plantings each of two native oak species (*Quercus lobata* and *Q. wislizenii*) were grown from seed

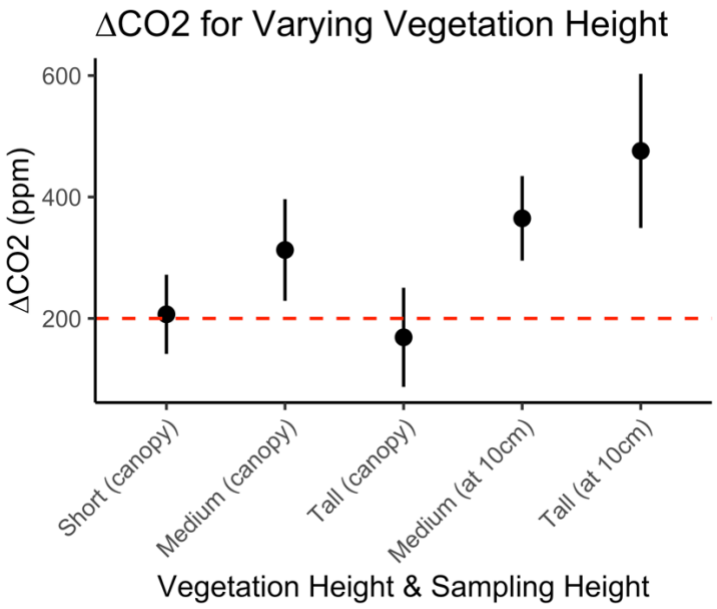

Fig. 2.7: *Mean and standard deviation of CO_2 elevation achieved in plots with varying heights of vegetation: short (10 cm), medium (25–35 cm), and tall (50–60 cm).*

within the system's 16 growth plots (six seedlings per species per plot), planted directly into the soil. The final surviving cohort of 128 seedlings was harvested in November 2023 (and is evaluated in Chapter 3). The next iteration of the TinyFACE system is being used to grow six species of native and exotic California grasses (*Brachypodium distachyon, Bromus hordeaceus, Elymus glaucus, Festuca californica, Festuca myuros,* and *Nasella pulchra*). Future investigations with TinyFACE include a developing study of eCO_2 effects on Arctic soil methane fluxes (D. Sirivat, personal communication).

4. Discussion

Our testing of TinyFACE has demonstrated that the system is capable of achieving a consistent CO_2 elevation of +200 ppm above ambient values with high precision and accuracy. Control is achieved with reference to air samples from a single plot, but all eCO_2 plot means fall within ± 34–38 ppm of the target elevation. Elevated CO_2 level is largely consistent within each plot and attenuates almost fully within 50 cm of the encircling screens, preventing any "leakage" of CO_2 to neighboring plots (1 m away). In the vertical dimension, control remains excellent at all points at or below the height of the enclosing screen.

TinyFACE achieves the treatment goal without requiring growth chambers or open-topped chambers to enclose the plants. Even with the minimal screen enclosure featured by the design,

microclimate effects are not insignificant, but the system nonetheless improves the realism of plant growth responses in climate change experiments when compared to other methods. The natural temperature patterns, rooting depths, day/night cycles, seasonality and weather regimes make results from this field-based method more trustworthy in predicting the responses of species and ecosystems to climate change. One way to address the temperature and shading effects caused by the screens would be to replace the greenhouse plastic with 100% transparent plexiglass or a similar material.

Study	**Leadley (1997)**	**Bindi (2001)**	**Okada (2001)**	**Miglietta (2001)**	**Messerli (2015)**	**Fangemeier (2016)**	**Wohlfahrt (2018)**	**TinyFACE (2024)**
Design	SACC	FACE	FACE	FACE	OTC	FACE	FACE	SACC
Plants	grasses	grapes	rice	bog ecosystem	alfalfa/timothy	wheat	grapes	oaks, grasses
Overnight	Y	N	Y	N	Y	Y	N	N
eCO_2 Replicates	20	4	4	5	4	5	3	8
Area/rep (m^2)	1.27	20	113	0.785	1.2	4	113	0.5
Total eCO_2 Area (m^2)	25.4	80	452	3.925	4.8	20	339	4
CO_2 Set [Obs]	650 ppm [600]	625 ppm [624]	570 ppm [570]	560 ppm [560]	600 ppm [632]	553 ppm [546]	500 ppm [476]	619 ppm [629]
ΔCO_2	237	253	199	189	232	143	68	210
Temporal Control: ±20% of target (±10%)	100% (92.2%)	84.10%	90% (60%)	95%	93% (66%)	93% (73%)		100% (96.9%)
CO_2 Usage (kg m^{-2} d^{-1})	6.1	–	4.88	4.74	3	3.16		2.62
Build Cost (2024 USD)	389,198	–	–	–	18,448	64416	–	14500
Build Cost (ppm^{-1} m^{-2})	64.65				16.57	22.52		17.29

Table 2.2: *Comparison of performance and design for eCO_2 experiments on short-stature plants.*

One of the primary goals in designing our system was to ensure high quality CO_2 control while minimizing costs. Table 2.2 lists performance and cost metrics for seven studies with comparable CO_2 elevation goals. TinyFACE fell near the middle of the pack in terms of desired elevation, and as the name implies, it had the smallest total area of eCO_2 treatment. Nonetheless, TinyFACE had the best temporal control, the lowest operational CO_2 consumption, and the second-lowest cost of construction, in terms of CO_2 elevation achieved on a per-area basis. Though not all studies reported construction costs, TinyFACE

cost just over one-fourth the price to build compared to its predecessor (Leadley et al. 1997), and only 4% more than the cheapest option we examined, an OTC system (Messerli et al. 2015). The required supply of CO_2 for TinyFACE is low compared to prior studies, on a per-time and per-area basis: between 1.64 and 2.62 kg CO_2 $m^{-2}d^{-1}$ is lower than the 3 kg CO_2 $m^{-2}d^{-1}$ required for a similar-sized OTC experiment (Messerli et al. 2015), and less than half the 6.1 kg CO_2 $m^{-2}d^{-1}$ required by the original SACC design (Leadley et al. 1997).

4.1 Limitations

Though its performance is promising, there are a number of limitations to this method of CO_2 enrichment. We conducted exploratory tests on the effects of vegetation height on CO_2 control, and caution that plants that will grow higher than the screen height of 43 cm may require a modified size and scaling of the plot volume. We recommend regular (e.g. monthly) adjustment of the *MFCbase* value to ensure the control algorithm is appropriate to the current stage of vegetation growth. This change, as well as adding or removing eCO_2 units to the system, will affect the rate of CO_2 consumption by the experiment as a whole.

Delivery of CO_2 from the tank to the plots is well regulated, but delivery of the tanks themselves to the experimental site proved quite a challenge at times during our preliminary study on oak seedlings. Our field site was located near CA Highway 128, which collapsed in several places during the winter storms of 2023. The driveway from the road to the experimental site developed a large sink-hole, and deliveries were impossible for several weeks. In more remote sites, access to CO_2 may prove an even greater challenge. Investigators might meet this challenge by installing a bulk CO_2 storage tank at their site, to increase storage capacity and reduce the number of delivery visits required.

After being built and calibrated, TinyFACE can run on its own for the most part, but it does require some routine monitoring and maintenance. We recommend recalibrating the gas analyzer once per month to prevent drift; regularly checking wiring, pump function, and screen integrity; and inspecting the system for leaks often. These duties can be performed during visits to tend to the plants grown in the array.

Data irregularities may require troubleshooting. Remote access to the data logger could allow researchers to set a threshold value of certain measurements that would indicate system malfunction. For example, unexpectedly high levels of ambient CO_2 may indicate a leak near the gas analyzer. A sudden synchrony between ambient, elevated, and the test sampling line's levels of CO_2 likely means the pump drawing air from the various sampling tubes is no longer working. Synchrony between just two of the three lines might mean a faulty connection in one of the solenoids or the eight-channel relays, meaning one of the three valves is permanently closed, and residual air from the previous sample is being measured.

In our pilot study, we aimed for ΔCO_2 values of +200 ppm, but we believe the TinyFACE system is capable of significantly higher elevation. In fact, as we calibrated the system we had some difficulty keeping CO_2 elevation from overshooting that mark. The average flow of CO_2 through the mass flow controller (less than 4 L min^{-1}) was less than 25% of the MFC's full capacity. The system is therefore likely capable of supporting larger plot areas, more replicates, higher CO_2 elevation, or a combination thereof. In case a larger plot area is desired, researchers should determine how the ratio of screen height to plot width affect CO_2 control ability, and make requisite adjustments.

One advantage of creating many small plots of CO_2-enriched growing area is the potential for multi-factor treatment experiments. The high cost of traditional FACE studies makes it difficult to replicate eCO_2 treatments, let alone provide enough replicates for a secondary treatment variable (water, temperature, soil nutrient additions, etc.). The TinyFACE system could be applied to address a multitude of questions about plant growth and competition under changing environmental variables.

4.2 Conclusions

Traditional FACE experiments have led to major advances in the study of crop and plant responses to climate change, but they unfortunately are cost prohibitive to most investigative teams. By streamlining the system control and required instrumentation, we have designed and demonstrated the performance of a field-based eCO_2 research method that will be affordable to many more researchers

worldwide. We hope this method can be a resource for scientists seeking to gather empirical data on multi-factor climate change experiments on plants and ecosystems throughout the world.

Our prototype of TinyFACE was built with inexpensive materials suited to a low-cost, medium-duration experiment (1–2 years). It can also be adapted for more permanent studies and/or more inclement environments, e.g. through the replacement of wooden stakes and greenhouse plastic with metal frames and plexiglass panels. With site-specific modifications, TinyFACE could be adapted to serve as a repeated experiment across multiple ecosystems, or across a gradient of interest (elevation, aridity, soil type, etc.). At comparatively low cost, TinyFACE provides a method that could enable climate change research on plants as part of regionally or globally distributed collaborative experiments.

The promise of standardized, inexpensive ecosystem experiments used in coordinated distributed experiments has been demonstrated for other ecosystem manipulations. Nutrient Network (Borer et al. 2014) and Drought-Net (Knapp et al. 2017) are two examples of successful efforts to coordinate experimental macroecology research methods across massive spatial scales, by uniting the efforts of research teams following common protocols. Ecosystem responses to climate change are highly variable, and empirical data is an essential complement to ecosystem climate models. As an affordable, quickly constructed, highly effective eCO_2 system, TinyFACE is a tool for climate researchers worldwide to apply to pressing ecological questions.

Chapter 3: The rich get richer: Future CO_2 levels are more beneficial to well-watered seedlings of native California oaks

Abstract

Elevated CO_2 (eCO_2) can change how plants respond to water stress. As human activities continue to increase atmospheric levels of CO_2, the well-studied patterns of physiology, growth, and morphology in water-stressed plants therefore may not hold true under future climates. To understand how plants and ecosystems might respond to water stress under the CO_2 levels expected for the mid-to-late 21st Century, we subjected oak tree seedlings to a full-factorial treatment of eCO_2 and watering over the course of 18 months. We tested the hypothesis that eCO_2 would mitigate realized water stress in the seedlings via reduced stomatal conductance and related improvements in water use efficiency, and that therefore plants in the low watering treatment would show greater growth enhancement under eCO_2 than would well-watered plants.

Acorns of two species (*Quercus lobata* and *Q. wislizeni*) were planted directly in the soil in a field-based miniature free-air CO_2 enrichment system. The seedlings were continuously subjected to ambient (415 ppm) or elevated CO_2 (550 ppm), and two watering treatments, in a full-factorial, replicated design. We found that instead of mitigating plant water stress, eCO_2 was most beneficial to well-watered *Q. wislizeni* seedlings, and it therefore widened rather than narrowing the performance gap caused by the watering treatment. *Q. lobata* seedlings in the experiment were heavily grazed by rodents, but their tendency to resprout after complete stem removal showed a similar response to the treatments: eCO_2 marginally increased resprouting rates, for well-watered seedlings only. These results imply that in near-future climates, vital plant processes like photosynthesis, growth, and resprouting will be more dependent on abundant soil water than they are now. Our results show the importance of multi-factor experiments to provide a mechanistic understanding of complex plant responses to the influences of climate change.

Key words: Climate change, water stress, *Quercus*, FACE, plant physiology

1. Introduction

Water stress is one of the biggest challenges to global forests today (Anderegg et al. 2020), and plants must balance demands for both water and CO_2 as they regulate their physiology (Haworth et al. 2013). Climate change is predicted to dramatically alter soil water and precipitation patterns (Cook et al. 2018), potentially shifting entire ecosystems towards more aridity-adapted communities, but plant responses to water stress itself are also likely to change under higher atmospheric CO_2 concentrations. As atmospheric CO_2 rises (Gulev et al. 2021), the negative impacts of water stress in plants may be reduced or altered by higher concentrations of CO_2 (Cernusak et al. 2019, Ainsworth and Long 2021) Because extra CO_2 can reduce transpirational water losses (Medlyn et al. 2001, Xu et al. 2016) and enhance photosynthetic uptake (Long et al. 2004), it is widely thought to promote plant water use efficiency, defined as the ratio of CO_2 gained to water lost during photosynthesis (Cernusak et al. 2019). For this reason alone, plant-water relations inferred from studies conducted at ambient CO_2 levels may not be a reliable predictor of future plant responses.

A nuanced, empirically validated understanding of tree responses to coincident changes in water and CO_2 is therefore necessary, not just to anticipate outcomes for individual trees and tree species, but also to characterize the feedback between forests and climate at a global scale. Free Air CO_2 Enrichment (FACE) and similar methods enable the study of elevated CO_2 (eCO_2) effects on trees in field settings, avoiding the pot and chamber effects and altered microclimates of laboratory and greenhouse studies (Kimball 2016). However, most field-based eCO_2 research in trees has focused on CO_2 as a single-factor treatment (Way et al. 2015, Ainsworth and Long 2021), and the number of studies that have examined its interaction with water have shown mixed results (Wullschleger et al. 2002, Duursma et al. 2011, Norby et al. 2016, Ainsworth and Long 2021) and often species-dependent outcomes (Kimball 2016, Bendall et al. 2022, O'Connor et al. 2022). Our full-factorial eCO_2 and watering treatment study took place in a field-based FACE system in the blue oak woodlands of California's Inner Coast Range. Our goal was to study whether seedlings of two native California oaks respond differently to water stress when grown under projected future CO_2 levels.

eCO_2 has been shown to affect plants in a variety of ways, most of which have implications for plant responses to water stress. The water savings mechanism (Gray et al. 2016, Jiang et al. 2021) is said to occur when eCO_2 causes lower stomatal conductance and therefore lower transpiration, reducing water losses to the environment. Water savings may increase net CO_2 uptake over the course of a season by enabling the plant to maintain photosynthesis further into a progressive drought (Ainsworth and Long 2021). On the other hand, eCO_2 can directly stimulate photosynthesis by hastening the reaction rate of Rubisco (Ainsworth and Rogers 2007, Leakey et al. 2009, Gray et al. 2016), thereby increasing net gain of CO_2. This extra CO_2 may in turn provide more biomass to allocate to root systems for enhanced water uptake (Ainsworth and Rogers 2007). In summary, eCO_2 can affect water use efficiency by reducing water loss, increasing CO_2 uptake, and/or by achieving one of these effects via the other.

If eCO_2 primarily alleviates water stress, one might expect to see an interaction between eCO_2 and watering treatments, such that the impact of abundant watering is less pronounced for eCO_2-treated plants. If, by contrast, increased net CO_2 uptake overwhelms changes to plant water status, then the effects of watering may be even *more* pronounced for eCO_2-treated plants, as extra CO_2 can only be taken advantage of if the plant has sufficient water to perform extra photosynthesis (Duan et al. 2013). The two mechanisms may both operate to some degree within a single system, either concurrently or in sequence; e.g. eCO_2-driven water savings may be achieved at moderate levels of water stress, but prevented under extreme water stress by stomatal closure (Duan et al. 2013) or temperature stress (Davis et al. 2007).

Early FACE studies on woody crops seemed to indicate that eCO_2 would alleviate drought stress (Kimball et al. 1995, Ainsworth and Long 2005), and indeed several studies since have found that eCO_2 effects are especially or only observed in trees experiencing water stress or drought conditions. Stomatal conductance, which is generally reduced by eCO_2, can be more strongly affected by eCO_2 in water-stressed trees (Medlyn et al. 2001). eCO_2 treatments can "rescue" trees from the decreased photosynthetic rates and leaf starch contents that water stress causes under ambient CO_2 concentrations (O'Connor et al. 2022). And eCO_2 can serve as an aid to establishment for oak seedlings in particular, increasing survival in the first years for seedlings in hot, dry conditions by counteracting the effects of their unfavorable

microclimate (Davis et al. 2007). These findings suggest that eCO_2 provides some water savings or otherwise mitigates water stress effects.

In recent years, however, the evidence for eCO_2 interactions with plant and soil water status has been less conclusive, and a number of results have found no evidence that eCO_2 mitigates the effects of water stress. Many studies have found that only well-watered plants experience growth and biomass increases under eCO_2, indicating that while eCO_2 can provide a benefit to plants, it does not necessarily counteract the negative effects of water stress. In fact, water stress can curtail the positive effects of eCO_2 on plant biomass (Bendall et al. 2022), and improvements in water use efficiency associated with eCO_2 can be negligible in comparison to drought-related declines in photosynthesis (Nackley et al. 2018). It may be that water stress is just as severe at eCO2 as at ambient levels.

One reason for the lack of consistency in these results may be that whole-plant responses like rooting depth or canopy leaf area can counterbalance or overwhelm leaf-level physiological effects of water and eCO_2 (Duursma et al. 2011, Purcell et al. 2018, Jiang et al. 2021), or that early-season changes to plant structures under eCO_2 can prove maladaptive under later-season drought (Gray et al. 2016). Furthermore, studies incorporating top-down influences, like fire, herbivory, and competition, have shown that eCO_2 effects on plant water status can be outweighed by factors at a broader ecological scale (Collins et al. 2018, Raubenheimer et al. 2021, Raubenheimer and Ripley 2022), meaning that leaf- and plant-level results should not be interpreted entirely out of context.

Several species of California oaks have been considered under threat of regeneration failure for at least a century (Tyler et al. 2006), and dramatic changes to patterns of fire and herbivory have affected the survival rates of oak seedlings, saplings, and resprouting shoots (Tyler et al. 2006, Arévalo et al. 2009), leading to demographic instability (Zavaleta et al. 2007). Climate change effects, including rising CO_2 levels and changing water regimes, may alter the critical establishment window for oak seedlings and other woody plants in grassland ecosystems (Davis et al. 2007, Nackley et al. 2018, Bendall et al. 2022). The influence of these multiple climate stressors on the vulnerable seedling life stage could determine the future of these trees and the ecosystems they form.

Plant responses to water stress and eCO_2 can almost all be traced back to changes in photosynthesis, stomatal conductance, or their combination (Long et al. 2004), but the downstream effects of these physiological processes include changes to the size, shape, and function of plants and their organs. In addition to shifts in their CO_2 uptake levels, plants may also change their allocation and the morphology of their organs based on water status, due to a shifting balance of key resources (Poorter and Ryser 2015). Accordingly, in our 2 × 2 factorial eCO_2 and watering treatment experiment, we examined nine plant response variables representing physiology, biomass, and morphology and allocation (Table 1) to provide a whole-plant perspective on the future of native California oak seedlings. Based on the hot, seasonally dry Mediterranean climate in which they thrive, we anticipated that eCO_2 would alleviate water stress in the seedlings via the water savings effect. We therefore predicted that the performance gap between well-watered and under-watered seedlings (in metrics like photosynthetic rate and biomass accumulation) would be reduced at elevated CO_2.

Variable	**Units**	**Description**
A_{net}	µmol m^2 s^{-1}	net photosynthetic uptake of CO_2
gs	mol m^2 s^{-1}	stomatal conductance of water
WUE	µmol/mol	water use efficiency: A_{net}/gs
total mass	g	mass of all plant tissues
root mass	g	mass of belowground tissues
final height	mm	height of main stem
total leaf area	mm^2	sum of leaf area per plant
root-to-shoot	g/g	ratio of root mass to aboveground tissues (stems and leaves)
SRL	mm/g	specific root length

Table 3.1: *Plant response variables studied.*

2. Methods

2.1 Study Site

This study was conducted using the tinyFACE CO_2 enrichment system (see Chapter 2). The research took place at Quail Ridge Reserve of the University of California Natural Reserve System, in

Napa County, CA, which features blue oak (*Quercus douglasii*) woodlands as well as associations of valley oak (*Q. lobata*) and live oak (*Q. wislizeni*). The experiment was located next to the Researcher House, on the eastern side of the ridge, at 365 m elevation. Since 2017, average precipitation at the site is 44.8 cm per year; the two water years immediately preceding our study were drier than this average (63.6 and 36.4% of average cumulative rainfall). In the first year of our study the site recorded 85.3% of the average, while the second winter was wetter than average (156.5% of average). Average temperatures for the past seven years are 8ºC in January and 28ºC in July (UC NRS). Rainfall and temperature data for the study period are available in supplementary figures (Fig. S3.1). Eighteen months before our study began (i.e. in August 2020), the site burned at moderate severity during the Hennessey Fire, a part of the LNU Lightning Complex.

2.2 Planting

The eCO_2 × watering treatment was applied to oak seedlings of two species (interior live oak, *Quercus wislizeni*, and valley oak, *Q. lobata*) in a randomized complete block design. Sixteen 0.5-m^2 circular treatment plots were arranged in a square around the central CO_2 enrichment system. Each of the four treatment levels (aCO_2+under-watered; aCO_2+well-watered; eCO_2+under-watered; eCO_2+well-watered) was represented once on each side of the square. As such, each side of the square represented a block, and each treatment level had four replicates in total.

In each treatment plot, 12 acorns of each species were planted directly in the soil in a single planting day in February 2022. *Q. wislzeni* seeds came from Devil Mountain Nursery in San Joaquin County, CA (collected October 2021 from a nursery collection), and *Q. lobata* seeds came from a private residence in Marin County, CA (collected October 2021 from a single source tree). Before planting, each seed was float-tested in water to check for viability, then dried and cleaned with 70% ethanol.

Using a 14 × 40 cm soil drill, twelve evenly spaced holes (7.5 cm wide × 15 cm deep) were made in each treatment plot. Half the holes were designated for *Q. wislizeni* and half for *Q. lobata* in a randomly interspersed pattern. Then, two acorns of one species were planted 1.5 cm below the soil

surface at each location, with their long axis parallel to the soil surface. After planting, each plot was encircled with 0.6 cm mesh hardware cloth to prevent seed loss to granivorous wildlife.

Of 384 seeds planted, 192 germinated (49.2% overall; 63.5% *Q. wislizeni*, 34.4% *Q. lobata*), with nearly all plots showing their first germinants by April 25, 2022. (Germination rates were not tested as a treatment response because CO_2 treatment and differential watering treatments had not yet begun at this point.) Forty-six seedlings were hand-thinned in August 2022 to avoid duplicates at each planting location, leaving a total of 143 experimental plants, of which 16 died before harvesting. Plots were hand-weeded throughout the experiment, as were the areas immediately outside the plot areas.

2.3 CO_2 Treatment

This experiment featured the first experimental application of the tinyFACE system. Chapter 2 provides a detailed description of its method of CO_2 elevation. In brief, each growth plot was surrounded by a perforated pipe blowing either ambient or CO_2-enriched air. A 45 cm screen helped maintain CO_2 concentrations while a 10 cm gap at the base of the screen allowed for turbulent mixing and minimized microclimate effects within the plot area (Leadley et al. 1997). A central blower provided air flow to the whole experiment, and CO_2 injection was controlled by a proportional-integral algorithm designed to maintain CO_2 elevation at +200 ppm. During the entire 18-month period of the experiment, including periods of maintenance, malfunction, or insufficient CO_2 supply, the median level of CO_2 elevation was +155 ppm (mean +127 ppm, sd = 79.3) (Fig. S3.2). CO_2 was administered at two treatment levels, ambient and elevated, but the concentrations achieved at each plot varied slightly, as determined by testing conducted in October 2023 (Fig. S3.3). CO_2 treatment began on March 26, 2022, before any seedlings had emerged. CO_2 elevation was more or less continuous after May 16, 2022, although the system required fine-tuning and calibration throughout the first year of the experiment. The system was designed to shut off the flow of CO_2 overnight (i.e. when PAR fell below 50 W m^{-2}).

2.4 Watering Treatment

Differential water status was achieved by applying supplemental water to the well-watered treatment group, starting in the second summer of the experiment. In the first summer of the experiment

(starting in May 2022), to aid in seedling establishment, all plots were hand-watered once per month (appx. 9.5 L). In August 2022, a drip irrigation system was installed for better saturation of the soil and lower evaporative loss. One-quarter-inch perforated tubing was placed in a serpentine pattern between the rows of seedlings in each plot, ensuring each seedling was exposed to the same number of outlet holes (18 total per plot). On one watering date each in August, September, and October of 2022, all plots were exposed to 60-90 minutes of drip irrigation (at 0.5 gph). During the winter months, no supplemental water was applied. In June 2023, an automated watering timer was installed to begin the differential watering treatment: well-watered plants received a small amount of drip irrigation daily, while under-watered plants did not. The daily irrigation was 5 min at 6:00:00 (June–July 2023), then 7 min at 15:30:00 (August–October 2023). The daily irrigation time was shifted to the afternoon when it was discovered that rodents, drawn to the water resource provided by the drip lines, were damaging the seedlings and the irrigation lines themselves, and that rodent activity peaked in the early morning (see further notes below). The under-watered plants also received 30 minutes of drip irrigation in early July, 2023, to prevent losses to drought-induced mortality.

2.5 Data Collection

Each plant was measured during plant growth inventories, which occurred eight times throughout the 18 months of the experiment. Data recorded at each inventory included height (measured to shoot apical meristem), stem diameter (taken at soil surface), and condition (a qualitative score from 1-5, with 5 being full health and 1 being dead).

Photosynthesis data were collected during sampling campaigns in August and September, 2023, using a Li-COR LI-6400 XT Portable Photosynthesis System (LI-COR, Inc.; Lincoln, NE). All measurements took place between 10:00:00 and 16:30:00. PAR was set to 1500 μmol $m^{-2}s^{-1}$, block temperature to 30ºC, and leaf fan speed to "fast." Photosynthetic rate (A_{net}, in μmol CO_2 m^{-2} s^{-1}) and stomatal conductance (g_s, in mol m^{-2} s^{-1}) were measured for one leaf on each plant. The three-step measurement protocol subjected the leaf to three levels of externally forced ambient CO_2 concentration (Ca): 400 ppm, 600 ppm, and 800 ppm, with each step lasting 120–240s. IRGA matching was performed

automatically after each step. The two surveys collected sufficient photosynthesis data for analysis of 72 plants. Soil water content of each plot was recorded immediately before taking photosynthesis measurements, using a time domain reflectometry probe (FieldScout TDR 150; Spectrum Technologies, Bridgend, UK) with 12 cm tines, taking the average of four readouts per plot within the planting area.

After the final photosynthesis survey and the last growth inventory concluded, the seedlings were harvested. Above-ground tissues were collected in late November 2023: leaves were separated from stems and stems were cut at their base, at the soil surface. Leaf tissues were immediately placed in plastic bags and transferred to a cooler to preserve their moisture content. Both tissue types were weighed on a mass balance, and the leaves were oven-dried at 65ºC for 36h, reaching a constant weight before having their mass measured and recorded. Roots were harvested in late January 2024, by digging a hole adjacent to the root of interest and then separating the exposed root from the soil matrix. Roots were washed immediately upon extraction, air dried for several weeks, and weighed on the mass balance.

Leaves and roots were photographed against a white background using an iPhone 6 SE camera. The resulting images were processed in ImageJ to create a black-and-white outline of the root or leaf in question. The prepared root images were further processed in RhizoVision Explorer (Seethepalli et al. 2021) to analyze root size, shape, and morphology. Settings for analysis were as follows: broken root mode; root prune threshold = 7; edge smoothing = 1; filter non-root objects = 1 mm^2; root diameter range threshold = 2.10 mm, for two total classes. Leaf area data were extracted directly from ImageJ.

2.6 Herbivory

Starting in July of 2023, we noticed a number of stems had been visibly gnawed or completely bitten through. On July 19, the hardware cloth cages around the plots were reinforced in an attempt to prevent further losses. Starting in July, and throughout the rest of the experiment, the first dates of observed herbivory were recorded. Herbivory primarily affected *Q. lobata* (chi-squared test, $p << 0.001$) and was associated with watering treatment (affecting the well-watered seedlings, $p < 0.002$); there was no significant association with CO_2 treatment ($p = 0.83$).

In total, 50 seedlings sustained herbivory damage, with 41 of those suffering completely severed stems. Thirty-four of these completely severed seedlings partially regrew or showed signs of resprouting, but were nonetheless excluded from further analysis involving stem or leaf mass as a response variable.

2.7 Data Analysis

The photosynthesis data collected for each plant were used to determine relationships between ambient CO_2 concentration (Ca), intercellular CO_2 concentration (Ci), and net CO_2 uptake by the plant (A_{net}). For each seedling, a linear model was used to predict Ci from Ca based on the data collected with the photosynthesis system (average $R^2 = 0.92$), and to derive the Ci value expected for the plot-specific mean CO_2 concentrations. The collected data were used to create a second linear model predicting A_{net} from Ci for each plant (average $R^2 = 0.80$), allowing the interpolation of a predicted A_{net} for the Ci expected at the treatment CO_2 concentration. A similar interpolation was performed for stomatal conductance (g_s), with a third and final linear model predicting g_s from the treatment Ci (average $R^2 = 0.61$). These A_{net} and g_s values represent the inferred photosynthetic and stomatal conductance rates achieved by the plants at their respective ambient CO_2 concentrations. Since time of day was found to be a significant predictor for both A_{net} and g_s, time of day (rescaled from 0 to 1) was included as a predictor in the models for A_{net}, and g_s (see below).

In addition to the data directly recorded, and the interpolated photosynthesis data described above, analyses included plant response variables derived from transformations or ratios of these previously described data types:

Total plant mass (g) = root mass (g) + stem mass (g) + leaf mass (g)

Root-to-shoot ratio (g/g) = root mass (g) / (stem mass (g) + leaf mass, fresh (g))

Specific root length (mm/g) = total root length (mm) / root mass (g)

Water use efficiency (WUE) (µmol CO_2/mol H2O) = A_{net}/ g_s

This study sought to examine the effects of water, eCO_2, and their interaction on plant physiology, size, morphology, and leaf water status. To assess these effects, we first examined the treatment effects on a categorical basis (well-watered or under-watered, aCO_2 or eCO_2). For each response variable, we converted the data to z-scores, then calculated bootstrap means and standard errors (1000 replicates) of the change observed with the addition of watering. We did this first for the aCO_2 plants, then for the eCO_2 plants, and compared the results to provide an overview of treatment effects and interactions. These values were taken as the means of all observations, rather than as per-plot means, to provide more informative standard errors. Additionally, photosynthesis variables were not time-corrected in this part of the analysis.

To provide more insight into the individual response variables, we fit multiple linear regressions or linear mixed-effects regressions for each plant response variable, making separate models for each species (Table S1, Table S2). To increase statistical power, the predictor variables used were continuous, rather than categorical: (1) percent soil water content (SWC) recorded for each plot, either at the time of LiCOR surveys, or as the average of all SWC measurements throughout the study, and (2) the CO_2 concentration recorded in each plot during testing on October 9, 2023, rescaled to fit the experiment-wide mean elevation of +127 ppm for eCO_2 plots. Since the predictor variables had meaningfully different units (percent soil water content vs. ppm CO_2), each was rescaled between 0 and 1 before modeling (though they are represented in their original units in illustrative figures, for ease of interpretation). This approach is useful because it means that the coefficients in the linear model can be interpreted as the difference in a given response variable between the lowest and highest level of the treatment variable in question. A third predictor variable, time of day rescaled from 0 to 1, was included for the photosynthesis-related models.

We examined a total of nine plant responses (Table 1). Since CO_2 and watering treatments were applied at the plot level, our analyses for most variables focused on the per-plot average of plant response variables for each species, to avoid pseudoreplication. Because observations for photosynthesis-related variables needed to be associated with a specific time of day, we instead opted to use mixed-effects

models fit by maximum likelihood with "Plot" as a random effect for A_{net}, g_s, and WUE. For the model of A_{net} for *Q. wislizeni*, the mixed-effects model exhibited singular fit, so for this species the A_{net} model was fit on per-plot means with time-of-observation averaged per plot as well.

A likelihood ratio test (from the R package lmtest) was used to choose between the full model (~ SWC × CO_2), the reduced model (~ SWC + CO_2), and the null model (~ 1 or ~ 1|Plot) for each response variable (with each species analyzed separately). The coefficients of the resulting models were then assessed for significance based on the t-statistic. Each model's residuals were checked for non-normality (Shapiro-Wilk test, all $p > 0.05$) and visually assessed to ensure homoscedasticity of variance using the qqPlot and qqmath functions in R.

Due to the high rate of herbivory on *Q. lobata* seedlings, we conducted an analysis of post-grazing resprouting rates for this species under the various treatments, using a general linear model for resprouting as a binomial response variable.

3. Results

We examined the effects of watering, eCO_2, and their interaction on a range of plant responses representing physiology, biomass, and morphology. Overall, seedlings of both species showed significant responses to watering treatment and eCO_2 as main effects. Furthermore, the interaction between watering and eCO_2 was a significant predictor in the photosynthetic rate, final height, specific root length of *Q. wislizeni*, meaning that the effect of watering changed at higher levels of ambient CO_2. The interaction between treatments approached significance as a predictor of post-grazing resprouting rates in *Q. lobata*.

The standardized effect size of responses to watering (i.e. change in z scores, expressed in units of standard deviations for the variable in question) ranged from a decrease of 0.92 sd (root-to-shoot ratio at aCO_2) to an increase of 1.61 sd (A_{net} at eCO_2) for *Q. lobata*, and from a decrease of 1.06 sd (root-to-shoot at aCO_2) to an increase of 1.48 sd (final height at aCO_2) for *Q. wislizeni* (Fig. 3.1). The largest difference in watering effects between eCO2 and aCO2 treatments was +0.65 sd for *Q. lobata* (for leaf area) and 0.83 sd for *Q. wislizeni* (A_{net}).

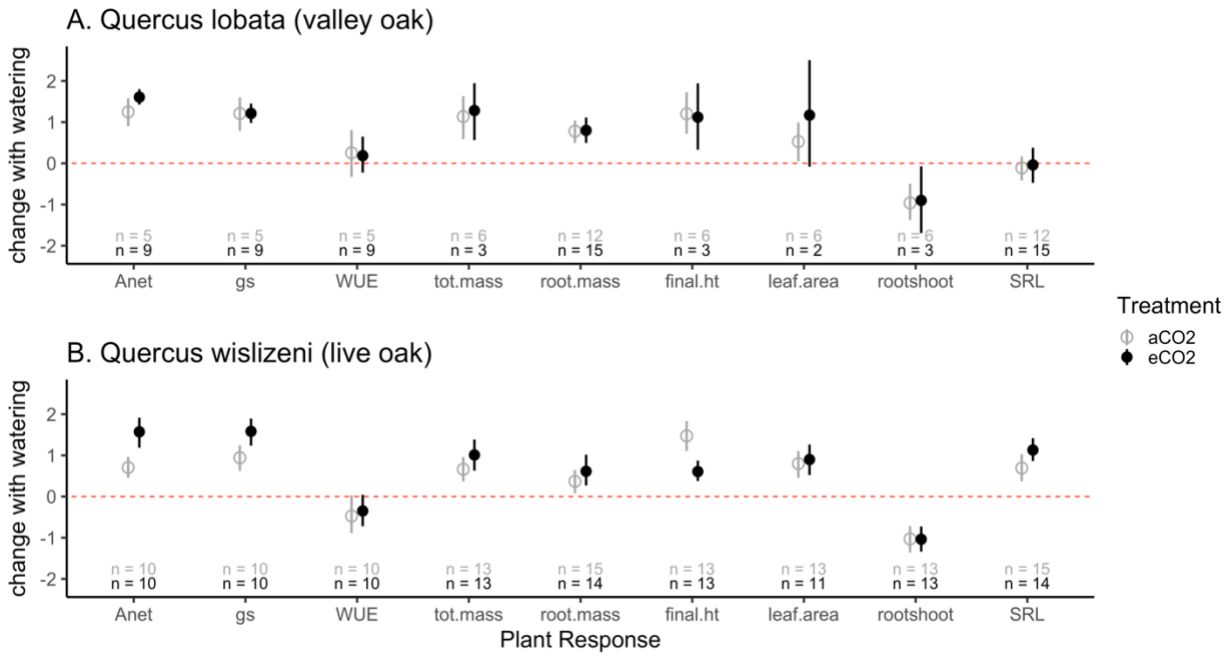

Fig. 3.1*: Standardized (z-score) change with watering, for various plant response variables: photosynthetic rate (A_{net}), stomatal conductance (g_s), water use efficiency (WUE), total biomass (tot.mass), belowground biomass (root.mass), stem height at harvest (final.ht), total leaf area per plant (leaf.area), root-to-shoot-ratio (rootshoot), specific root length (SRL). The effect of watering is calculated as the difference in z-score for well-watered - under-watered treatment, using a bootstrap sampling of each distribution (R = 1000). Points represent mean ± bootstrap se. Sample sizes represent the lower of the two watering treatments for each CO_2 treatment.*

We developed models for each of the nine plant responses under the additive or interacting effects of eCO_2 (Table S1, Table S2). We highlight the following results. β terms represent the slope of linear regression, or the change in the given response variable from the minimum to the maximum level of soil water treatment (or CO_2 treatment) for main effects. In the case of interaction, they represent the *difference* in slope for the effect of SWC given the maximum applied eCO_2.

3.1 Physiology

For *Q. lobata*, photosynthetic rate and stomatal conductance both increased significantly with watering (β = 16.0 μmol $m^{-2}s^{-1}$, t = 5.98, p << .001; β = 0.22 mol $m^{-2}s^{-1}$, t = 6.88, p << .001), and decreased with time of day (β = -7.93 μmol $m^{-2}s^{-}$, t = -2.74, p = 0.0097; β = -0.15 mol $m^{-2}s^{-1}$, t = -3.96, p << .001), while only photosynthetic rate responded to eCO_2 (β = 9.81 μmol $m^{-2}s^{-}$, t = 3.55, p = 0.0044). WUE did not change significantly in response to either treatment, although it had a marginal positive association with eCO_2 (β = 34.3, t = 1.79, p = .098).

For *Q. wislizeni*, photosynthesis showed a strong interacting effect of the watering and CO_2 treatments ($\beta = 11.27$ µmol CO_2 $m^{-2}s^{1}$, $t = 2.55$, $p = 0.027$), indicating that eCO_2 caused a greater increase in A_{net} for well-watered seedlings than for dry seedlings (Fig. 3.2a). Stomatal conductance increased significantly with watering ($\beta = 0.091$ mol $m^{-2}s^{-1}$, $t = 6.98$, $p << .001$), and showed an unexpected increase in response to eCO_2 which approached significance ($\beta = 0.023$ mol $m^{-2}s^{-1}$, $t = 1.72$, $p = 0.11$) WUE didn't change significantly for this species as a result of the treatments or their interaction (all $p > 0.17$).

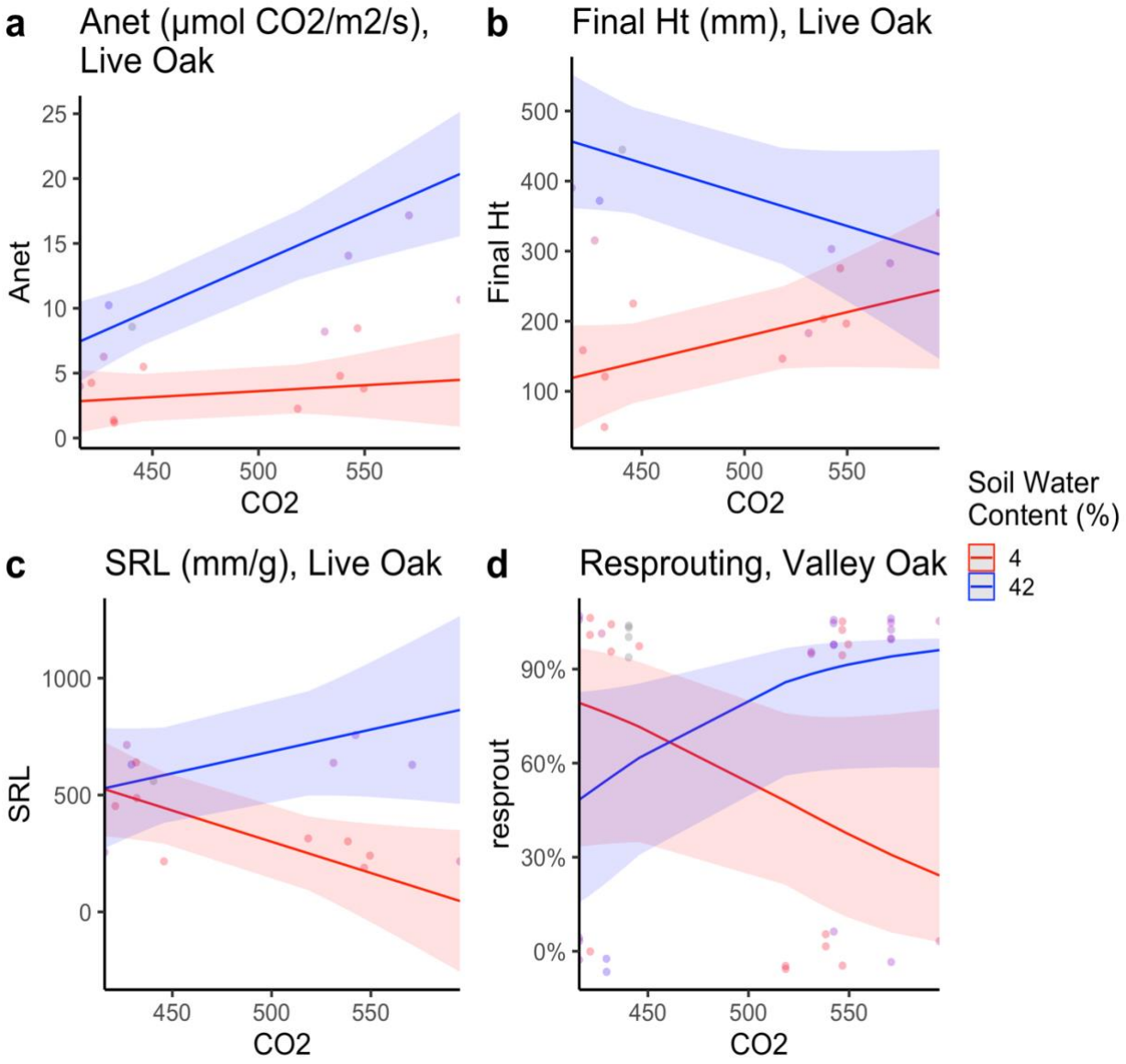

Fig. 3.2 *Linear models and per-plot means for photosynthetic rate in Q. wislizeni (a), final height in Q. wislizeni (b), specific root length in Q. wislizeni (c), and resprouting in Q. lobata (d).*

3.2 Biomass

Of the biomass variables, final height and total biomass increased significantly in response to the watering treatment for *Q. lobata* (height: β = 245.6 mm, t = 2.87, p = 0.024; total biomass: β = 10.9 g, t = 3.13, p = 0.017), but not in response to eCO_2. (A positive effect of eCO_2 on total biomass, β = 6.1 g, approached significance, with t = 1.93, p = 0.10.) Root mass, the only biomass variable whose sample size was not impacted by data losses due to grazing, showed positive response to eCO_2 (β = 2.53 g, t = 2.26, p = 0.041) as well as water (β = 2.30 g, t = 2.11, p = 0.055).

The *Q. wislizeni* seedlings in the study displayed an increase in total biomass and leaf area in response to watering treatment (biomass: β = 9.99 g, t = 2.69, p = 0.018; leaf area: β = 10516 mm^2, t = 2.27, p = 0.041), though root mass for this species was not significantly affected by either watering or eCO_2 (p = 0.12 and 0.13). The final height of the seedlings was positively influenced by watering for all seedlings, but the height increase provided by watering was smaller at eCO_2 than at aCO_2 (β = -286.58 mm, t = -2.05, p = 0.063) (Fig. 3.2b, Fig. 3.3).

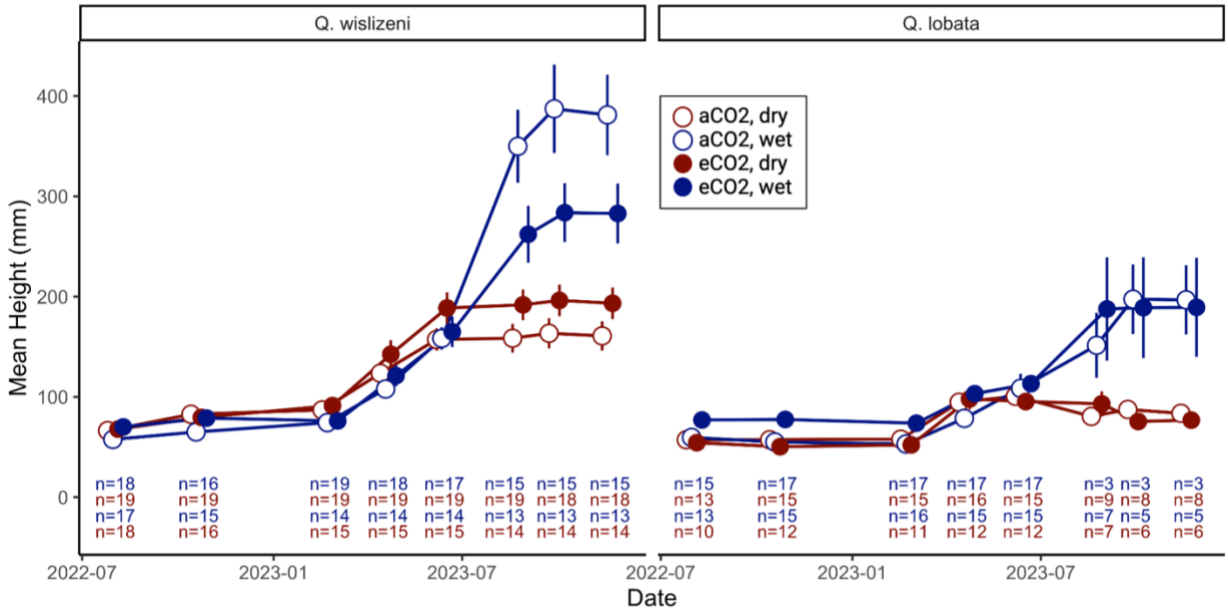

Fig. 3.3 *Seedling heights measured throughout the study, showing mean heights (± se) per treatment group: red = under-watered, blue = well-watered; open circles = aCO2, filled circles = eCO2. Starting in July 2023, seedlings damaged by herbivores were excluded from the totals.*

3.3 Morphology

Watered *Q. lobata* seedlings on average allocated less biomass to their root systems (root-to-shoot ratio: $\beta = -1.30$, $t = -1.87$, $p = 0.10$), as did watered seedlings of *Q. wislizeni* ($\beta = -0.31$, $t = -3.34$, $p = 0.005$). The data showed no relationship between the treatments and specific root length (mm of root per g of root mass) for *Q. lobata*, but an interaction between watering and eCO_2 was demonstrated for this variable in *Q. wislizeni* seedlings: watering increased specific root length for all seedlings, but provided a greater increase to seedlings under eCO_2 ($\beta = 813.40$ mm/g, $t = 2.17$, $p = 0.051$) (Fig. 3.2c).

3.4 Resprouting

The interaction of watering and eCO_2 improved resprouting rates in previously grazed *Q. lobata* seedlings, in an effect that approached significance ($\beta = 5.74$, $z = 1.78$, $p = 0.075$) (Fig. 3.3d).

4. Discussion

In synoptic terms, our expectation that eCO_2 would alleviate the effects of water stress was not met for either species. We proposed that eCO_2 would increase A_{net} and decrease stomatal conductance more strongly for under-watered plants, leading the under-watered plants to demonstrate greater improvements in biomass under eCO_2. In fact, *Q. wislizeni* showed an interaction effect with the opposite sign: rather than helping water-stressed plants make up the difference, eCO_2 increased the performance gap between well-watered and under-watered seedlings (Fig. 3.1a).

Q. lobata showed no significant interaction effects in the responses studied, but from a small sample of grazed seedlings, we found an intriguing suggestion that resprouting rates are positively associated with the interaction between watering and eCO_2 (Fig. 3.2d).

For *Q. wislizeni*, the increase in A_{net} under full watering depended strongly on CO_2 treatment, as we expected, but it was stronger for the eCO_2 rather than the aCO_2 seedlings (Fig. 3.2a). That result was reflected in the mean responses of total mass and root mass for this species (Fig. 3.1b), though not to a degree that met the threshold of statistical significance (Table S3.2). Our finding is consistent with several other studies (Nackley et al. 2018, Bendall et al. 2022, Gardner et al. 2022), which in sum indicate support for the "direct stimulation" mechanism of eCO_2 effects on angiosperm trees or tree seedlings. Past

a certain point of water stress, plants cannot maintain open stomata, and so water-stressed plants may be unable to fix enough of the extra CO_2 regardless of higher concentration (Duan et al. 2013). Well-watered plants, by contrast, receive a stronger benefit from eCO_2 to the degree that their stomata are able to stay open more and longer, allowing CO_2 fixation to increase along with ambient concentrations (Bendall et al. 2022).

We were surprised by the positive (though non-significant) stomatal response each species showed to eCO_2 (Table S3.1, Table S3.2). The majority of results from FACE research indicate that eCO_2 leads to decreased stomatal conductance for most species (Medlyn et al. 2001, Ainsworth and Long 2021, Mndela et al. 2022), providing the basis for improved WUE, and by extension, the foundation of most plant benefits from eCO_2 under the water savings mechanism (Long et al. 2004, Jiang et al. 2021). The finding that stomatal conductance actually *increased* under eCO_2 for both species was unusual, though not unique. A recent FACE study on grape vines found increased stomatal conductance under eCO_2 (Wohlfahrt et al. 2018), and in spite of mean reductions in stomatal conductance, the major FACE studies of the past three decades indicate that 12% of stomatal conductance changes are in fact positive (Purcell et al. 2018). Stomatal models have shown that under certain combinations of temperature and water stress, increased stomatal conductance under eCO_2 is the optimum response (Purcell et al. 2018). Additionally, eCO_2-related reductions in stomatal conductance early in the season could save soil water that actually leads to an increase in later-season stomatal conductance, compared to aCO_2 plants nearby which have already run out of soil water reserves after a long, dry summer.

Q. wislizeni seedling heights showed different responses to watering, depending on CO_2 treatment: while both groups increased in height in response to watering, the aCO_2 plants' height increase was much larger (Fig. 3.2b, Fig. 3.3 left panel). However, the change in stem height was not accompanied by a change in stem mass—there was no significant effect of any of the treatments on stem mass as a proportion of total plant mass ($p = 0.77$, data not shown). The seedlings changed the shape of their stems, rather than the mass of carbon allocated towards stem tissues. Although many studies indicate that eCO_2 leads to increased height for plants (Raubenheimer and Ripley 2022), the reverse finding is not unheard

of. In a CO_2 × drought experiment on *Eucalyptus saligna*, eCO_2-grown trees were significantly shorter than their ambient-CO_2 counterparts, contrary to expectations and for unknown reasons (Duursma et al. 2011). For the *Q. wislizeni* seedlings in this study, both outcomes were observed, since the well-watered seedlings were shorter under eCO_2 treatment, while under-watered seedlings under eCO_2 were taller (Fig. 3.3, left panel). Since plants have more plasticity in the morphology of their organs than in the allocation of carbon (Poorter and Ryser 2015), this type of change may be an important component of plant response to climate. The resulting pattern meant that, under CO_2 levels expected within this century, the height advantage conferred by abundant soil water was significantly reduced.

Changes in root morphology under watering also depended on CO_2: while specific root length did not differ strongly by watering treatment at aCO_2, well-watered plants at eCO_2 increased their specific root length and under-watered plants at eCO_2 decreased it (Fig. 3.2c). A decrease in specific root length indicates shorter, thicker roots, but *Q. wislizeni* did not show significant changes in absolute root mass; once again, the shape of the organ, not its mass, was shown to be most responsive (Poorter and Ryser 2015). Decreased specific root length provides greater penetrative force in hard soil (Pérez-Harguindeguy et al. 2013). Lower specific root length therefore has a logical advantage for seedlings under water stress, especially in the hard, clay-heavy soils of Quail Ridge Reserve (Lambert and Kashiwagi 1978). It is unclear why eCO_2 should be necessary to trigger this change, as it requires no additional carbon allocation.

Q. lobata seedling responses to eCO_2 and watering treatment demonstrated little to no interaction effect: responses to watering were not significantly different based on CO_2 treatment. The loss of up to 85% of observations per treatment group for this species due to small mammal grazing made it difficult to make meaningful inferences about some responses for *Q. lobata*.

Though herbivory was not one of our intended treatments of interest, a field-based, ecologically relevant setting meant the plants in this study experienced certain stressors that are present in the real world. Herbivory itself can change with exposure to eCO_2: leaf-eating insects can increase consumption under eCO_2 for many reasons, including lower N content of leaves (Bezemer and Jones 1998); increased

plant secondary compounds (O'Neill et al. 2010); or canopy temperature increase related to decreased stomatal conductance (Dermody et al. 2008). In our study, herbivory was not significantly associated with eCO_2, but as it was not an intended component of the experiment, we cannot rule out an effect of CO_2 on herbivory rates. It was abundantly clear that the rodents in question were preferentially feeding on plants from the well-watered treatment; we cautiously interpret this pattern to be related to the experimental artifact of drip irrigation, which the rodents sought out as a water source during times of extreme dry weather at the site (Fig. S3.1), rather than the quality of the plant tissues themselves.

Further experiments to specifically study eCO_2 effects on herbivory and resprouting rates in this system may be useful in light of the intensity of the grazing we observed. Other studies have indicated that herbivory can outweigh growth benefits of eCO_2 (Collins et al. 2018), and at Quail Ridge, the extremely high grazing rates on young oaks have been shown to negate the competitive advantage conferred on oak species with strong post-fire resprouting (Arévalo et al. 2009). Grazing and fire are both important filters on community assembly in California's oak woodlands (Arévalo et al. 2009), and it is possible that future CO_2 levels will affect seedling resilience to these local drivers via effects on resprouting. Past research has indicated an enhancement of resprouting for tree seedlings under eCO_2, due to larger belowground C storage tissues (Bendall et al. 2022). Herbivory was not associated with treatment groups, but at least for *Q. lobata*, post-grazing resprouting rates may have been influenced by the interaction of watering and eCO_2 (Fig. 3.2d). If the advantage of abundant soil water to resprouting rates is only realized at eCO_2, this may be another way in which near-future climates widen the gap between water-stressed and well-watered oak seedlings.

4.1 Conclusion

The results show that we were correct in our prediction of a significant interaction of eCO_2 and water stress, albeit with different sign than expected. The A_{net} results for *Q. wislizeni* and the resprouting rates for *Q. lobata* present new empirical evidence that the eCO_2 levels of the future may only benefit those plants with sufficient water resources. This information is necessary for accurate climate predictions, as well as for forecasting the fate of individual species and ecosystems. *Q. wislizeni* also

demonstrated plasticity in root and shoot morphology responses to eCO_2 and water. Though our methods did not provide a complete framework for understanding the implications of the observed CO_2-dependent height and specific root length response to watering, they provide interesting avenues for further study.

While many of the results for *Q. lobata* were hindered by data loss to rodents, the fact of its susceptibility to herbivory is an interesting result in itself. The felled seedlings and gnawed irrigation tubes were a useful reminder that plant life exists in the context of a larger ecosystem. Even as they balanced CO_2 and water needs, these oak seedlings were subject to the broader-scale challenges of an ecosystem that was *itself* responding to changes in climate and resource availability. Our results provide new insights into the seedling life stage for two oak species, a cautionary tale about the threat of small rodents, and novel results showing the mechanisms of plant responses to climate change.

Chapter 3 Supplemental Figures

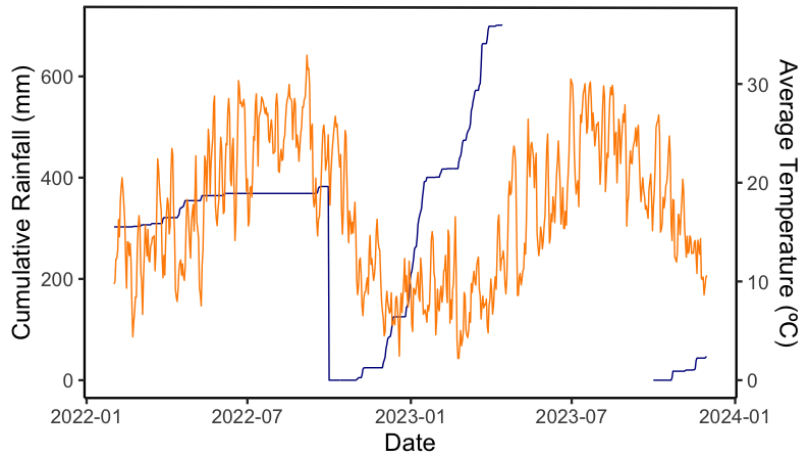

Fig. S3.1: *Cumulative rainfall and average daily temperature at Quail Ridge Reserve.*

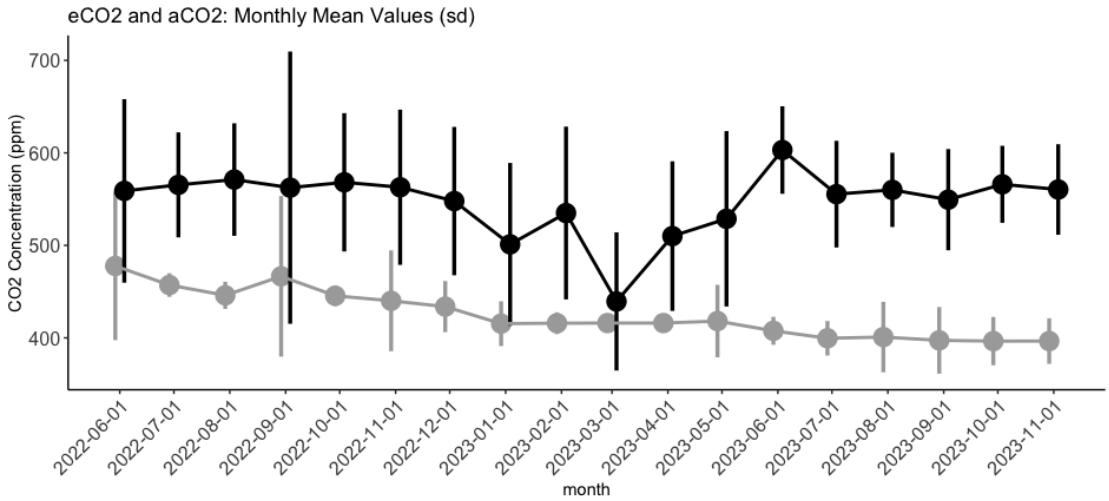

Fig. S3.2*: Mean (± sd) CO_2 elevation achieved by the tinyFACE system for the duration of the study.*

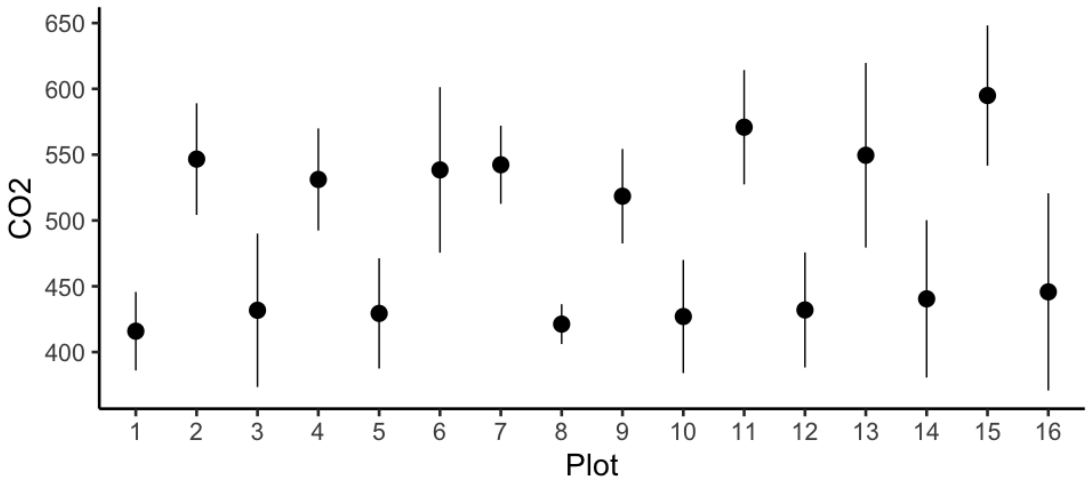

Fig. S3.3*: Spatial control of tinyFACE system, showing CO_2 levels per plot as tested on October 9, 2023.*

Valley Oak (*Quercus lobata*)

	Estimate	Std. Error	df	t value	p	
lmer(A_{net} ~ CO2 + SWC + time + (1 | Plot))						
CO2	9.805	2.763	11.255	3.549	0.00441	**
SWC	15.99	2.673	12.782	5.982	4.91E-05	***
time	-7.936	2.892	32.956	-2.744	0.00973	**
lmer(gs ~ CO2 + SWC + time + (1 | Plot))						
CO2	0.04862	0.03341	14.5	1.455	0.166903	
SWC	0.22335	0.03248	15.82	6.876	3.96E-06	***
time	-0.146	0.03689	32.48	-3.96	0.000384	***
lmer(WUE ~ CO2 + SWC + time + (1 | Plot)						
CO2	34.32	19.13	11.85	1.793	0.09843	.
SWC	-22.39	18.75	12.04	-1.194	0.25541	
time	33.76	24.07	27.06	1.403	0.1721	
lm(tot.mass ~ CO2 + SWC)						
CO2	6.053	3.136		1.93	0.0949	.
SWC	10.892	3.475		3.134	0.0165	*
lm(root.mass ~ CO2 + SWC)						
CO2	2.527	1.116		2.263	0.04138	*
SWC	2.304	1.093		2.108	0.05503	.
lm(final.ht ~ CO2 + SWC)						
CO2	80.21	77.17		1.039	0.3332	
SWC	245.59	85.51		2.872	0.0239	*
lm(leaf.area ~ CO2 * SWC)						
CO2	-2765	5609		-0.493	0.6479	
SWC	-3006	5696		-0.528	0.6255	
CO2:SWC	25368	16483		1.539	0.1986	
lm(rootshoot ~ CO2 + SWC)						
CO2	-0.1221	0.6242		-0.196	0.85	
SWC	-1.2959	0.6916		-1.874	0.103	
lm(SRL ~ CO2 + SWC)						
CO2	-60.39	115.65		-0.522	0.61	
SWC	-25.25	113.23		-0.223	0.827	

Table S3.1*: Plant response models for Q. lobata. Models shown in gray were outscored by the null model.*

Interior Live Oak (*Quercus wislizeni*)

	Estimate	Std. Error	df	t value	p	
lm(A_{net} ~ CO2 * SWC + time)						
CO2	1.639	2.317		0.707	0.49419	
SWC	4.608	1.963		2.348	0.03863	*
time	-3.687	1.84		-2.004	0.07029	.
CO2:SWC	11.266	4.42		2.549	0.02705	*
lmer(gs ~ CO2 + SWC + time + (1|Plot), REML = F)						
CO2	0.0226	0.01316	16.02319	1.718	0.10507	
SWC	0.09066	0.01299	20.26837	6.981	8.30E-07	***
time	-0.03873	0.01676	22.5331	-2.312	0.0303	
lmer(WUE ~ CO2 + SWC + time + (1 | Plot), REML = F)						
CO2	30.341	21.581	9.775	1.406	0.191	
SWC	-22.152	19.657	15.975	-1.127	0.276	
time	15.953	24.294	21.206	0.657	0.518	
lm(tot.mass ~ CO2 + SWC)						
CO2	5.45	3.79		1.438	0.1741	
SWC	9.993	3.711		2.693	0.0184	*
lm(root.mass ~ CO2 + SWC)						
CO2	2.413	1.511		1.597	0.1343	
SWC	2.461	1.479		1.664	0.12	
lm(final.ht ~ CO2 * SWC)						
CO2	125.48	73.25		1.713	0.112388	
SWC	337.52	61.96		5.447	0.000148	***
CO2:SWC	-286.58	139.62		-2.053	0.062592	.
lm(leaf.area ~ CO2 + SWC)						
CO2	4224	4738		0.891	0.38887	
SWC	10516	4639		2.267	0.04111	*
lm(rootshoot ~ CO2 + SWC)						
CO2	0.02871	0.09393		0.306	0.76472	
SWC	-0.30744	0.09197		-3.343	0.00529	**
lm(SRL ~ CO2 * SWC)						
CO2	-478.366	196.948		-2.429	0.031797	*
SWC	4.044	166.597		0.024	0.981032	
CO2:SWC	813.396	375.407		2.167	0.051095	.

Table S3.2: Plant response models for *Q. wislizeni*.

Bibliography

Agee, J. K. 1996. The Influence of Forest Structure on Fire Behavior. Pages 52–68 Proceedings of the 17th Forest Vegetation Management Conference. Redding, CA.

Ainsworth, E. A., and S. P. Long. 2005. What have we learned from 15 years of free-air CO2 enrichment (FACE)? A meta-analytic review of the responses of photosynthesis, canopy properties and plant production to rising CO2. New Phytologist 165:351–372.

Ainsworth, E. A., and S. P. Long. 2021. 30 years of free-air carbon dioxide enrichment (FACE): What have we learned about future crop productivity and its potential for adaptation? Global Change Biology 27:27–49.

Ainsworth, E. A., and A. Rogers. 2007. The response of photosynthesis and stomatal conductance to rising [CO2]: mechanisms and environmental interactions. Plant, Cell & Environment 30:258–270.

Akima, H. 1978. A Method of Bivariate Interpolation and Smooth Surface Fitting for Irregularly Distributed Data Points. ACM Transactions on Mathematical Software 4:148–159.

Anderegg, W. R. L., A. T. Trugman, G. Badgley, C. M. Anderson, A. Bartuska, P. Ciais, D. Cullenward, C. B. Field, J. Freeman, S. J. Goetz, J. A. Hicke, D. Huntzinger, R. B. Jackson, J. Nickerson, S. Pacala, and J. T. Randerson. 2020. Climate-driven risks to the climate mitigation potential of forests. Science 368:eaaz7005.

Arévalo, J. R., P. Álvarez, N. Narvaez, and K. Walker. 2009. The effects of fire on the regeneration of a Quercus douglasii stand in Quail Ridge Reserve, Berryessa Valley (California). Journal of Forest Research 14:81–87.

Baddeley, A., R. Turner, and E. Rubak. 2024, July 15. spatstat: Spatial Point Pattern Analysis, Model-Fitting, Simulation, Tests.

Bendall, E. R., M. Bedward, M. Boer, H. Clarke, L. Collins, A. Leigh, and R. A. Bradstock. 2022. Growth enhancements of elevated atmospheric [CO2] are reduced under drought-like conditions in temperate eucalypts. Functional Ecology 36:1542–1558.

Bezemer, T. M., and T. H. Jones. 1998. Plant-Insect Herbivore Interactions in Elevated Atmospheric CO2: Quantitative Analyses and Guild Effects. Oikos 82:212–222.

Bindi, M., L. Fibbi, M. Lanini, and F. Miglietta. 2001. Free Air CO_2 Enrichment (FACE) of grapevine (*Vitis vinifera* L.):: I.: Development and testing of the system for CO_2 enrichment. EUROPEAN JOURNAL OF AGRONOMY 14:135–143.

Borer, E. T., W. S. Harpole, P. B. Adler, E. M. Lind, J. L. Orrock, E. W. Seabloom, and M. D. Smith. 2014. Finding generality in ecology: a model for globally distributed experiments. Methods in Ecology and Evolution 5:65–73.

Brodie, E. G., E. E. Knapp, W. R. Brooks, S. A. Drury, and M. W. Ritchie. 2024. Forest thinning and prescribed burning treatments reduce wildfire severity and buffer the impacts of severe fire weather. Fire Ecology 20:17.

Brown, P., C. Gentry, B. Cassell, A. Dugan, J. Harris, C. King, J. Marschall, D. Pérez-Salicrup, G. Smith, and J. Waldron. 2010. Fire and recruitment history of a Jeffery pine stand in the eastern Sierra Nevada, California.

Bunn, A., M. Korpela, F. Biondi, F. Campelo, P. Mérian, F. Qeadan, C. Zang, A. Buras, A. Cecile, M. Mudelsee, M. Schulz, S. Klesse, D. Frank, R. Visser, E. Cook, and K. Anchukaitis. 2024, June 1. dplR: Dendrochronology Program Library in R.

California Department of Forestry and Fire Protection. 2019, December 19. California Fire Perimeters (all). California State Geoportal.

Cernusak, L., V. Haverd, O. Brendel, D. Le Thiec, J.-M. Guehl, and M. Cuntz. 2019. Robust reponse of terrestrial plants to rising CO2. Trends in Plant Science.

Churchill, D. J., G. C. Carnwath, A. J. Larson, and S. A. Jeronimo. 2017. Historical forest structure, composition, and spatial pattern in dry conifer forests of the western Blue Mountains, Oregon.

Page PNW-GTR-956. U.S. Department of Agriculture, Forest Service, Pacific Northwest Research Station, Portland, OR.
Churchill, D., A. Larson, M. Dahlgreen, J. Franklin, P. Hessburg, and J. Lutz. 2013. Restoring forest resilience: From reference spatial patterns to silvicultural prescriptions and monitoring. Forest Ecology and Management 291:442–457.
Cline, S. P., A. B. Berg, and H. M. Wight. 1980. Snag Characteristics and Dynamics in Douglas-Fir Forests, Western Oregon. The Journal of Wildlife Management 44:773–786.
Collins, L., this link will open in a new window Link to external site, M. M. Boer, V. R. de Dios, S. A. Power, E. R. Bendall, S. Hasegawa, R. O. Hueso, J. P. Nevado, and R. A. Bradstock. 2018. Effects of competition and herbivory over woody seedling growth in a temperate woodland trump the effects of elevated CO2. Oecologia 187:811–823.
Cook, B. I., J. S. Mankin, and K. J. Anchukaitis. 2018. Climate Change and Drought: From Past to Future. Current Climate Change Reports 4:164–179.
Davis, M. A., P. B. Reich, M. J. B. Knoll, L. Dooley, M. Hundtoft, and I. Attleson. 2007. Elevated atmospheric CO_2 : a nurse plant substitute for oak seedlings establishing in old fields. Global Change Biology 13:2308–2316.
De Foliart, G. R. 2002. Insects Formerly Used as Food by Indigenous Populations of North America North of Mexico. Page The Human Use of Insects as a Food Resource. University of Wisconsin.
Dermody, O., B. F. O'Neill, A. R. Zangerl, M. R. Berenbaum, and E. H. DeLucia. 2008. Effects of elevated CO2 and O3 on leaf damage and insect abundance in a soybean agroecosystem. Arthropod-Plant Interactions 2:125–135.
Dolanc, C. R., H. D. Safford, J. H. Thorne, and S. Z. Dobrowski. 2014. Changing forest structure across the landscape of the Sierra Nevada, CA, USA, since the 1930s. Ecosphere 5:art101.
Duan, H., J. S. Amthor, R. A. Duursma, A. P. O'Grady, B. Choat, and D. T. Tissue. 2013. Carbon dynamics of eucalypt seedlings exposed to progressive drought in elevated [CO2] and elevated temperature. Tree Physiology 33:779–792.
Duursma, R. A., C. V. M. Barton, D. Eamus, B. E. Medlyn, D. S. Ellsworth, M. A. Forster, D. T. Tissue, S. Linder, and R. E. McMurtrie. 2011. Rooting depth explains [CO2] × drought interaction in Eucalyptus saligna. Tree Physiology 31:922–931.
Edelmann, P., W. W. Weisser, D. Ambarlı, C. Bässler, F. Buscot, M. Hofrichter, B. Hoppe, H. Kellner, C. Minnich, J. Moll, D. Persoh, S. Seibold, C. Seilwinder, E.-D. Schulze, S. Wöllauer, and W. Borken. 2023. Regional variation in deadwood decay of 13 tree species: Effects of climate, soil and forest structure. Forest Ecology and Management 541:121094.
Esri Community Maps Contributors. (n.d.). SoilWeb. UC Davis GIS.
Fangmeier, A., V. Torres-Toledo, J. Franzaring, and W. Damsohn. 2016. Design and performance of a new FACE (free air carbon dioxide enrichment) system for crop and short vegetation exposure. Environmental and Experimental Botany 130:151–161.
Fraver, S., J. B. Bradford, and B. J. Palik. 2011. Improving Tree Age Estimates Derived from Increment Cores: A Case Study of Red Pine:7.
Fry, D. L., S. L. Stephens, B. M. Collins, M. P. North, E. Franco-Vizcaíno, and S. J. Gill. 2014. Contrasting Spatial Patterns in Active-Fire and Fire-Suppressed Mediterranean Climate Old-Growth Mixed Conifer Forests. PLoS ONE 9:e88985.
Gardner, A., D. S. Ellsworth, K. Y. Crous, J. Pritchard, and A. R. MacKenzie. 2022. Is photosynthetic enhancement sustained through three years of elevated CO2 exposure in 175-year-old Quercus robur? Tree Physiology 42:130–144.
Gascho Landis, A. M., and J. D. Bailey. 2006. Predicting Age of Pinyon and Juniper Using Allometric Relationships. Western Journal of Applied Forestry 21:203–206.
Gill, S. J., G. S. Biging, and E. C. Murphy. 2000. Modeling conifer tree crown radius and estimating canopy cover. Forest Ecology and Management 126:405–416.
Girvetz, E. H., and S. E. Greco. 2007. How to define a patch: a spatial model for hierarchically delineating organism-specific habitat patches. Landscape Ecology 22:1131–1142.

Gray, S. B., O. Dermody, S. P. Klein, A. M. Locke, J. M. McGrath, R. E. Paul, D. M. Rosenthal, U. M. Ruiz-Vera, M. H. Siebers, R. Strellner, E. A. Ainsworth, C. J. Bernacchi, S. P. Long, D. R. Ort, and A. D. B. Leakey. 2016. Intensifying drought eliminates the expected benefits of elevated carbon dioxide for soybean. Nature Plants 2:16132.

Gucker, C. L. 2007. Pinus jeffreyi. U.S. Department of Agriculture, Forest Service, Rocky Mountain Research Station, Fire Sciences Laboratory.

Gulev, S. K., P. W. Thorne, J. Ahn, F. J. Dentener, C. M. Domingues, S. Gerland, D. Gong, D. S. Kaufman, J. Q. Nnamchi, J. A. Rivera, S. Sathyendranath, S. L. Smith, B. Trewin, K. von Schuckmann, and R. S. Vose. 2021. Changing State of the Climate System. Pages 287–422 *in* Intergovernmental Panel on Climate Change (IPCC), editor. Climate Change 2021: The Physical Science Basis. Contribution of Working Group I to the Sixth Assessment Report of the Intergovernmental Panel on Climate Change [Masson-Delmotte, V., P. Zhai, A. Pirani, S.L. Connors, C. Péan, S. Berger, N. Caud, Y. Chen, L. Goldfarb, M.I. Gomis, M. Huang, K. Leitzell, E. Lonnoy, J.B.R. Matthews, T.K. Maycock, T. Waterfield, O. Yelekçi, R. Yu, and B. Zhou (eds.)]. Cambridge University Press, Cambridge.

Hagmann, R. K., P. F. Hessburg, S. J. Prichard, N. A. Povak, P. M. Brown, P. Z. Fulé, R. E. Keane, E. E. Knapp, J. M. Lydersen, K. L. Metlen, M. J. Reilly, A. J. Sánchez Meador, S. L. Stephens, J. T. Stevens, A. H. Taylor, L. L. Yocom, M. A. Battaglia, D. J. Churchill, L. D. Daniels, D. A. Falk, P. Henson, J. D. Johnston, M. A. Krawchuk, C. R. Levine, G. W. Meigs, A. G. Merschel, M. P. North, H. D. Safford, T. W. Swetnam, and A. E. M. Waltz. 2021. Evidence for widespread changes in the structure, composition, and fire regimes of western North American forests. Ecological Applications 31:e02431.

Haworth, M., C. Elliott-Kingston, and J. C. McElwain. 2013. Co-ordination of physiological and morphological responses of stomata to elevated [CO2] in vascular plants. Oecologia 171:71–82.

Hijmans, R. J., R. Bivand, K. Dyba, E. Pebesma, and M. D. Sumner. 2024, May 22. terra: Spatial Data Analysis.

IPCC. 2021. Climate Change 2021 – The Physical Science Basis: Working Group I Contribution to the Sixth Assessment Report of the Intergovernmental Panel on Climate Change. First edition. Cambridge University Press.

Jiang, M., J. W. G. Kelly, B. J. Atwell, D. T. Tissue, and B. E. Medlyn. 2021. Drought by CO2 interactions in trees: a test of the water savings mechanism. New Phytologist 230:1421–1434.

Jones, A. G., J. Scullion, N. Ostle, P. E. Levy, and D. Gwynn-Jones. 2014. Completing the FACE of elevated CO2 research. Environment International 73:252–258.

Kimball, B. A. 2016. Crop responses to elevated CO2 and interactions with H2O, N, and temperature. Current Opinion in Plant Biology 31:36–43.

Kimball, B. A., P. J. Pinter, R. L. Garcia, R. L. LaMORTE, G. W. Wall, D. J. Hunsaker, G. Wechsung, F. Wechsung, and T. Kartschall§. 1995. Productivity and water use of wheat under free-air CO2 enrichment. Global Change Biology 1:429–442.

Knapp, A. K., M. L. Avolio, C. Beier, C. J. W. Carroll, S. L. Collins, J. S. Dukes, L. H. Fraser, R. J. Griffin-Nolan, D. L. Hoover, A. Jentsch, M. E. Loik, R. P. Phillips, A. K. Post, O. E. Sala, I. J. Slette, L. Yahdjian, and M. D. Smith. 2017. Pushing precipitation to the extremes in distributed experiments: recommendations for simulating wet and dry years. Global Change Biology 23:1774–1782.

Koontz, M. J., M. P. North, C. M. Werner, S. E. Fick, and A. M. Latimer. 2020. Local forest structure variability increases resilience to wildfire in dry western U.S. coniferous forests. Ecology Letters 23:483–494.

Kueppers, L. M., J. Southon, P. Baer, and J. Harte. 2004. Dead Wood Biomass and Turnover Time, Measured by Radiocarbon, along a Subalpine Elevation Gradient. Oecologia 141:641–651.

Lambers, H., F. S. C. III, and T. L. Pons. 2008. Plant Physiological Ecology. Springer Science & Business Media.

Lambert, G., and J. Kashiwagi. 1978. Soil survey of Napa County, California. US Natural Resource Conservation Service, Washington.
Larson, A. J., and D. Churchill. 2012. Tree spatial patterns in fire-frequent forests of western North America, including mechanisms of pattern formation and implications for designing fuel reduction and restoration treatments. Forest Ecology and Management 267:74–92.
Larsson, L.-Å. 2005. CDendro & CooRecorder program package.
Leadley, P. W., P. Niklaus, R. Stocker, and Ch. Körner. 1997. Screen-aided CO2 control (SACC): a middle ground between FACE and open-top chambers. Acta Oecologica 18:207–219.
Leakey, A. D. B., E. A. Ainsworth, C. J. Bernacchi, A. Rogers, S. P. Long, and D. R. Ort. 2009. Elevated CO2 effects on plant carbon, nitrogen, and water relations: six important lessons from FACE. Journal of Experimental Botany 60:2859–2876.
Lee, R. 2020, March. Morrill Act of 1862 Indigenous Land Parcels Database. High Country News.
Long, S. P., E. A. Ainsworth, A. Rogers, and D. R. Ort. 2004. Rising atmospheric carbon dioxide: plants FACE the future. Annual Review of Plant Biology 55:591–628.
Lydersen, J. M., M. P. North, E. E. Knapp, and B. M. Collins. 2013. Quantifying spatial patterns of tree groups and gaps in mixed-conifer forests: reference conditions and long-term changes following fire suppression and logging. Forest Ecology and Management 304:370–382.
Ma, Q., Y. Su, C. Niu, Q. Ma, T. Hu, X. Luo, X. Tai, T. Qiu, Y. Zhang, R. C. Bales, L. Liu, M. Kelly, and Q. Guo. 2023. Tree mortality during long-term droughts is lower in structurally complex forest stands. Nature Communications 14:7467.
Madley, B. 2016. An American Genocide: The United States and the California Indian Catastrophe, 1846-1873. Yale University Press.
van Mantgem, P. J., and N. L. Stephenson. 2007. Apparent climatically induced increase of tree mortality rates in a temperate forest. Ecology Letters 10:909–916.
McIntyre, P. J., J. H. Thorne, C. R. Dolanc, A. L. Flint, L. E. Flint, M. Kelly, and D. D. Ackerly. 2015. Twentieth-century shifts in forest structure in California: Denser forests, smaller trees, and increased dominance of oaks. Proceedings of the National Academy of Sciences 112:1458–1463.
Medlyn, B. E., C. V. M. Barton, M. S. J. Broadmeadow, R. Ceulemans, P. D. Angelis, M. Forstreuter, M. Freeman, S. B. Jackson, S. Kellomäki, E. Laitat, A. Rey, P. Roberntz, B. D. Sigurdsson, J. Strassemeyer, K. Wang, P. S. Curtis, and P. G. Jarvis. 2001. Stomatal conductance of forest species after long-term exposure to elevated CO2 concentration: a synthesis. New Phytologist 149:247–264.
Messerli, J., A. Bertrand, J. Bourassa, G. Bélanger, Y. Castonguay, G. Tremblay, V. Baron, and P. Seguin. 2015. Performance of Low-Cost Open-Top Chambers to Study Long-Term Effects of Carbon Dioxide and Climate under Field Conditions. Agronomy Journal 107:916–920.
Meyer, M. D., A. Wuenschel, and M. Slaton. 2019. Indiana Summit Research Natural Area Post- Fire Ecological Assessment.
Miglietta, F., M. R. Hoosbeek, J. Foot, F. Gigon, A. Hassinen, M. Heijmans, A. Peressotti, T. Saarinen, N. van Breemen, and B. Wallén. 2001. Spatial and Temporal Performance of the MiniFACE (Free Air CO2 Enrichment) System on Bog Ecosystems in Northern and Central Europe. Environmental Monitoring and Assessment 66:107–127.
Mndela, M., J. T. Tjelele, I. C. Madakadze, M. Mangwane, I. M. Samuels, F. Muller, and H. T. Pule. 2022. A global meta-analysis of woody plant responses to elevated CO2: implications on biomass, growth, leaf N content, photosynthesis and water relations. Ecological Processes 11:52.
Morrison, M. L., and M. G. Raphael. 1993. Modeling the Dynamics of Snags. Ecological Applications 3:322–330.
Nackley, L. L., A. Betzelberger, A. Skowno, A. G. West, B. S. Ripley, W. J. Bond, and G. F. Midgley. 2018. CO2 enrichment does not entirely ameliorate *Vachellia karroo* drought inhibition: A missing mechanism explaining savanna bush encroachment. Environmental and Experimental Botany 155:98–106.

Ng, J., M. P. North, A. J. Arditti, M. R. Cooper, and J. A. Lutz. 2020. Topographic variation in tree group and gap structure in Sierra Nevada mixed-conifer forests with active fire regimes. Forest Ecology and Management 472:118220.

Norby, R. J., M. G. D. Kauwe, T. F. Domingues, R. A. Duursma, D. S. Ellsworth, D. S. Goll, D. M. Lapola, K. A. Luus, A. R. MacKenzie, B. E. Medlyn, R. Pavlick, A. Rammig, B. Smith, R. Thomas, K. Thonicke, A. P. Walker, X. Yang, and S. Zaehle. 2016. Model–data synthesis for the next generation of forest free-air CO2 enrichment (FACE) experiments. New Phytologist 209:17–28.

North, M. P., B. M. Collins, and S. L. Stephens. 2012. Using fire to increase the scale, benefits and future maintenance of fuels treatments. Journal of Forestry. 110(7): 492-401 110:392–401.

North, M. P., K. M. Van de Water, S. L. Stephens, and B. M. Collins. 2009. Climate, Rain Shadow, and Human-Use Influences on Fire Regimes in the Eastern Sierra Nevada, California, USA. Fire Ecology 5:20–34.

O'Connor, R. C., D. M. Blumenthal, T. W. Ocheltree, and J. B. Nippert. 2022. Elevated CO2 counteracts effects of water stress on woody rangeland-encroaching species. Tree Physiology:tpac150.

Okada, M., M. Lieffering, H. Nakamura, M. Yoshimoto, H. Y. Kim, and K. Kobayashi. 2001. Free-air CO2 enrichment (FACE) using pure CO2 injection: system description. New Phytologist 150:251–260.

Oksanen, J., G. L. Simpson, F. G. Blanchet, R. Kindt, P. Legendre, P. R. Minchin, R. B. O'Hara, P. Solymos, M. H. H. Stevens, E. Szoecs, H. Wagner, M. Barbour, M. Bedward, B. Bolker, D. Borcard, G. Carvalho, M. Chirico, M. D. Caceres, S. Durand, H. B. A. Evangelista, R. FitzJohn, M. Friendly, B. Furneaux, G. Hannigan, M. O. Hill, L. Lahti, D. McGlinn, M.-H. Ouellette, E. R. Cunha, T. Smith, A. Stier, C. J. F. T. Braak, and J. Weedon. 2024, May 21. vegan: Community Ecology Package.

O'Neill, B., A. Zangerl, E. Delucia, and M. Berenbaum. 2010. Olfactory Preferences of Popillia japonica , Vanessa cardui , and Aphis glycines for Glycine max Grown Under Elevated CO2. Environmental entomology 39:1291–301.

Pebesma, E., R. Bivand, E. Racine, M. Sumner, I. Cook, T. Keitt, R. Lovelace, H. Wickham, J. Ooms, K. Müller, T. L. Pedersen, D. Baston, and D. Dunnington. 2024, March 24. sf: Simple Features for R.

Pepin, S., and C. Körner. 2002. Web-FACE: a new canopy free-air CO2 enrichment system for tall trees in mature forests. Oecologia 133:1–9.

Pérez-Harguindeguy, N., S. Díaz, E. Garnier, S. Lavorel, H. Poorter, P. Jaureguiberry, M. S. Bret-Harte, W. K. Cornwell, J. M. Craine, D. E. Gurvich, C. Urcelay, E. J. Veneklaas, P. B. Reich, L. Poorter, I. J. Wright, P. Ray, L. Enrico, J. G. Pausas, A. C. De Vos, N. Buchmann, G. Funes, F. Quétier, J. G. Hodgson, K. Thompson, H. D. Morgan, H. Ter Steege, L. Sack, B. Blonder, P. Poschlod, M. V. Vaieretti, G. Conti, A. C. Staver, S. Aquino, and J. H. C. Cornelissen. 2013. New handbook for standardised measurement of plant functional traits worldwide. Australian Journal of Botany 61:167.

Petrie, M. D., R. M. Hubbard, J. B. Bradford, T. E. Kolb, A. Noel, D. R. Schlaepfer, M. A. Bowen, L. R. Fuller, and W. K. Moser. 2023. Widespread regeneration failure in ponderosa pine forests of the southwestern United States. Forest Ecology and Management 545:121208.

Plotkin, J. B., and H. C. Muller-Landau. 2002. Sampling the Species Composition of a Landscape. Ecology 83:3344–3356.

Poorter, H., F. Fiorani, R. Pieruschka, T. Wojciechowski, W. H. van der Putten, M. Kleyer, U. Schurr, and J. Postma. 2016. Pampered inside, pestered outside? Differences and similarities between plants growing in controlled conditions and in the field. New Phytologist 212:838–855.

Poorter, H., and P. Ryser. 2015. The limits to leaf and root plasticity: what is so special about specific root length? New Phytologist 206:1188–1190.

Purcell, C., S. P. Batke, C. Yiotis, R. Caballero, W. K. Soh, M. Murray, and J. C. McElwain. 2018. Increasing stomatal conductance in response to rising atmospheric CO2. Annals of Botany 121:1137–1149.
Pusina, T., P. Lackovic, and J. Moghaddas. 2023. Fire and Fuels Specialist Report, Eastern Sierra Climate and Communities Resilience Project. Page 51. Whitebark Institute.
Raubenheimer, S. L., and B. S. Ripley. 2022. CO2-stimulation of savanna tree seedling growth depends on interactions with local drivers. Journal of Ecology 110:1090–1101.
Raubenheimer, S. L., K. Simpson, R. Carkeek, and B. Ripley. 2021. Could CO2-induced changes to C4 grass flammability aggravate savanna woody encroachment? African Journal of Range & Forage Science 39:82–95.
Safford, H. D., and J. T. Stevens. 2017. Natural range of variation for yellow pine and mixed-conifer forests in the Sierra Nevada, southern Cascades, and Modoc and Inyo National Forests, California, USA. Page PSW-GTR-256. U.S. Department of Agriculture, Forest Service, Pacific Southwest Research Station, Albany, CA.
Sánchez Meador, A. 2024, February 8. Patch Delineation Package.
Sánchez Meador, A. J., P. F. Parysow, and M. M. Moore. 2011. A New Method for Delineating Tree Patches and Assessing Spatial Reference Conditions of Ponderosa Pine Forests in Northern Arizona. Restoration Ecology 19:490–499.
Seethepalli, A., K. Dhakal, M. Griffiths, H. Guo, G. T. Freschet, and L. M. York. 2021. RhizoVision Explorer: open-source software for root image analysis and measurement standardization. AoB PLANTS 13:plab056.
Slaton, M. R., J. G. Holmquist, M. Meyer, R. Andrews, and J. Beidl. 2019. Traditional Ecological Knowledge Used in Forest Restoration Benefits Natural and Cultural Resources: The Intersection between Pandora Moths, Jeffrey Pine, People, and Fire. Natural Areas Journal 39:461–471.
Speer, J. 2010. Fundamentals of Tree Ring Research. University of Arizona Press.
Stephens, S. L., D. E. Foster, J. J. Battles, A. A. Bernal, B. M. Collins, R. Hedges, J. J. Moghaddas, A. T. Roughton, and R. A. York. 2024. Forest restoration and fuels reduction work: Different pathways for achieving success in the Sierra Nevada. Ecological Applications 34:e2932.
Stevens, J. T. 2017. Scale-dependent effects of post-fire canopy cover on snowpack depth in montane coniferous forests. Ecological Applications 27:1888–1900.
Stokes, M. A. 1968. An introduction to tree-ring dating. University of Chicago Press, Chicago.
Swann, A. L. S., F. M. Hoffman, C. D. Koven, and J. T. Randerson. 2016. Plant responses to increasing CO2 reduce estimates of climate impacts on drought severity. Proceedings of the National Academy of Sciences of the United States of America 113:10019–10024.
Swetnam, T. W., C. D. Allen, and J. L. Betancourt. 1999. APPLIED HISTORICAL ECOLOGY: USING THE PAST TO MANAGE FOR THE FUTURE. Ecological Applications 9:18.
Taylor, A. H., and C. B. Halpern. 1991. The structure and dynamics of *Abies magnifica* forests in the southern Cascade Range, USA. Journal of Vegetation Science 2:189–200.
Taylor, A. H., V. Trouet, C. N. Skinner, and S. Stephens. 2016. Socioecological transitions trigger fire regime shifts and modulate fire–climate interactions in the Sierra Nevada, USA, 1600–2015 CE. Proceedings of the National Academy of Sciences 113:13684–13689.
Taylor, D. W. 1982. Ecological Survey of the vegetation of lndiana Summit Research Natural Area, Inyo National Forest, California.
Tomiolo, S., M. A. Harsch, R. P. Duncan, P. E. Hulme, S. Tomiolo, M. A. Harsch, R. P. Duncan, and P. E. Hulme. 2016. Influence of climate and regeneration microsites on Pinus contorta invasion into an alpine ecosystem in New Zealand. AIMS Environmental Science 3:525–540.
Tyler, C. M., B. Kuhn, and F. W. Davis. 2006. Demography and Recruitment Limitations of Three Oak Species in California. The Quarterly Review of Biology 81:127–152.
UC NRS. 2015, August 10. Quail Ridge Reserve. https://ucnrs.org/reserves/quail-ridge-reserve/.

Urgenson, L. S., C. R. Nelson, R. D. Haugo, C. B. Halpern, J. D. Bakker, C. M. Ryan, A. E. M. Waltz, R. T. Belote, and E. Alvarado. 2018. Social perspectives on the use of reference conditions in restoration of fire-adapted forest landscapes. Restoration Ecology 26:987–996.
U.S. DOE. 2020. U.S. Department of Energy Free-Air CO2 Enrichment Experiments: FACE Results, Lessons, and Legacy. U.S. Department of Energy Office of Science.
USGCRP. 2018. Fourth National Climate Assessment. Pages 1–470. U.S. Global Change Research Program, Washington, DC.
Van de Water, K. M., and H. D. Safford. 2011. A Summary of Fire Frequency Estimates for California Vegetation before Euro-American Settlement. Fire Ecology 7:26–58.
Wagtendonk, J. W. van, N. G. Sugihara, S. L. Stephens, A. E. Thode, K. E. Shaffer, and J. A. Fites-Kaufman, editors. 2018. Fire in California's Ecosystems. Second edition.
Way, D. A., R. Oren, and Y. Kroner. 2015. The space-time continuum: the effects of elevated CO2 and temperature on trees and the importance of scaling. Plant, Cell & Environment 38:991–1007.
Williams, J. W., and S. T. Jackson. 2007. Novel climates, no-analog communities, and ecological surprises. Frontiers in Ecology and the Environment 5:475–482.
Wohlfahrt, Y., K. Krüger, D. Papsdorf, S. Tittmann, and M. Stoll. 2022. Grapevine leaf physiology and morphological characteristics to elevated CO2 in the VineyardFACE (Free air Carbon dioxide Enrichment) experiment. Frontiers in Plant Science 13.
Wohlfahrt, Y., J. P. Smith, S. Tittmann, B. Honermeier, and M. Stoll. 2018. Primary productivity and physiological responses of *Vitis vinifera* L. cvs. under Free Air Carbon dioxide Enrichment (FACE). European Journal of Agronomy 101:149–162.
Woodward, F. I. 1987. Stomatal numbers are sensitive to increases in CO2 from pre-industrial levels. Nature 327:617–618.
Wullschleger, S. D., T. J. Tschaplinski, and R. J. Norby. 2002. Plant water relations at elevated CO2–implications for water-limited environments. Plant, Cell & Environment 25:319–331.
Xu, Z., Y. Jiang, B. Jia, and G. Zhou. 2016. Elevated-CO2 Response of Stomata and Its Dependence on Environmental Factors. Frontiers in Plant Science 7:657.
Zavaleta, E. S., K. B. Hulvey, and B. Fulfrost. 2007. Regional patterns of recruitment success and failure in two endemic California oaks. Diversity and Distributions 13:735–745.

Figures 2.1 and 2.2 were created with BioRender.com.